REPORT DOCUMENTATION PAGE

Form Approved OMB No. 0704-0188

1. AGENCY USE ONLY (Leave blank)	2. REPORT DATE	3. REPORT TYPE AND DATES COVERED
	14 Nov 00	Final Report

4. TITLE AND SUBTITLE

"Investigation of passive control devices applied to a launch vehicle structure to reduce the interior noise levels during launch"

5. FUNDING NUMBERS

F6256200M9068

6. AUTHOR(S)

Prof. Colin Hansen

7. PERFORMING ORGANIZATION NAME(S) AND ADDRESS(ES)

University of Adelaide
Dept. of Mechanical Engineering
Adelaide 5005
Australia

8. PERFORMING ORGANIZATION REPORT NUMBER

N/A

9. SPONSORING/MONITORING AGENCY NAME(S) AND ADDRESS(ES)

AOARD
UNIT 45002
APO AP 96337-5002

10. SPONSORING/MONITORING AGENCY REPORT NUMBER

AOARD-99-10

11. SUPPLEMENTARY NOTES

12a. DISTRIBUTION/AVAILABILITY STATEMENT

Approved for public release; distribution is unlimited.

12b. DISTRIBUTION CODE

A

13. ABSTRACT (Maximum 200 words)

The work discussed in the report is an extension of work undertaken by Dr. Steve Griffin of the Air Force Research Lab at Kirtland AFB, NM, during his participation in an AFOSR Windows on Science program at the University of Adelaide, South Australia in 1998. The previous work involved an investigation of the application of active feedback control of the launch vehicle structural vibration using radiation mode vibration levels as the cost function to minimize interior noise levels and led to the publication of three papers. The small benefit of action control, compared to the passive effect of the un-excited actuators attached to the structure has been the impetus behind the work conducted in the paper which is directed at optimizing the passive effect of vibration reducing devices.

The objectives of the study were achieved. A numerical framework for the study of the response of an irregularly shaped vibro-acoustic system excited by an external pressure field has been developed. The method used the modal coupling technique which coupled the in-vacuo modal model of the structure to the rigid –walled modal model of the cavity. The solution times of the (modal coupling) method were found to be extremely fast, solving two to three orders of magnitude faster than a fully coupled FEA. The modal coupling technique was validated against a fully coupled FEA. The FE model of the structure was adjusted so as to accurately emulate the physical structure. The effect of the VAD was analyzed and optimized for two bandwidths, namely 50-200Hz ands 50-400Hz . It was found that the optimal VAD design used the TMD as a highly reactive device to reduce the structural modal density within the frequency band of interest and the optimal diaphragm configuration was highly lossy to reduce the modal amplitude of the single acoustic mode. Local flexure of the panel reduced the effectiveness of the VAD's and alternative attachment techniques were investigated to reduce such flexure. The broadband noise reductions in the space averaged sound levels with the optimized VAD was 12dB.

14. SUBJECT TERMS			15. NUMBER OF PAGES 74
Acoustics			16. PRICE CODE N/A

17. SECURITY CLASSIFICATION OF REPORT	18. SECURITY CLASSIFICATION OF THIS PAGE	19. SECURITY CLASSIFICATION OF ABSTRACT	20. LIMITATION OF ABSTRACT
UNCLASSIFIED	UNCLASSIFIED	UNCLASSIFIED	UL

20010122 159

ADELAIDE
UNIVERSITY
AUSTRALIA

Investigation of Passive Control Devices for Potential Application to a Launch Vehicle Structure to Reduce the Interior Noise Levels During Launch

14th November 2000

Final Report for Stage 1

Prepared For: AFOSR

Contract Number: F6256200M9068

Prepared by: Professor Colin H. Hansen
Dr. Anthony C. Zander
Dr. Ben S. Cazzolato
Mr Rick C. Morgans
Department of Mechanical Engineering
The University of Adelaide SA 5005
AUSTRALIA
14th November 2000

Executive Summary

The worked discussed in the following report is an extension of the work undertaken by Dr Steve Griffin of the Air Force Research Lab at Kirtland AFB, New Mexico during his participation in the AFOSR Windows on Science program at the University of Adelaide, South Australia in 1998. The previous work involved an investigation of the application of active feedback control of the launch vehicle structural vibration using radiation mode vibration levels as the cost function to minimise interior noise levels and led to the publication of three papers. The small benefit of active control, compared to the passive effect of the un-excited actuators attached to the structure has been the impetus behind the work conducted here which is directed at optimising the passive effect of vibration reducing devices.

Within the report a numerical framework is developed for solving the response of a coupled vibro-acoustic system. It was decided to use a combination of *Modal Coupling Analysis* and *Finite Element Analysis* for the structure and internal cavities, with *Boundary Element Analysis* providing the solutions for the external pressure field. The modal coupling technique, which coupled the *in-vacuo* modal model of the structure to the rigid-walled modal model of the cavity, was found to have extremely fast solution times, solving two to three orders of magnitude faster than a fully coupled FEA. The modal coupling technique was validated against a fully coupled FEA.

The system under investigation was one used previously by Dr Griffin. It consisted of a 2.142m long, 6.35mm thick steel cylinder with an outside diameter of 0.514m. One end was capped with a rigid plywood end-cap, the other had a flexible aluminium panel with a thickness of 3.376mm. A FE model of the structure and the cavity was created. The parameters used for the model of the structure were adjusted so as to accurately emulate the experimental structure.

With the model and modelling technique validated, the various passive devices were investigated as can be seen in the table below. The empty cylinder provided a baseline by which to compare the results of the space averaged sound pressure level (acoustic potential energy) for two bandwidths, namely 50-200Hz and 50-400Hz. The equivalent mass of the Vibro-Acoustic Device (VAD) was smeared over the surface of the panel and the resultant sound field was calculated. The baseline Tuned Mass Device (TMD), which was essentially a mass and spring attached at three symmetric locations on the panel, was analysed. The effect of a passive Vibro-Acoustic Device (VAD) attached to the panel and coupled to the interior cavity was also evaluated. The VAD orientation was rotated to determine if the direction of the diaphragm had an influence on the VAD performance. Finally, the VAD was optimised. Two optimal cases are shown in the table below.

Case	Acoustic Potential Energy (dB)
Empty Cylinder	47.6 | 49.6
Equivalent Mass	35.9 | 36.6
TMD Baseline	28.8 | 51.3
VAD Baseline	30.1 | 51.4
Reversed VAD Baseline	29.3 | 50.7
Stiffened Seven Springs VAD	28.2 | 43.6
Stiffened Seven Springs VAD - Alternative spring arrangement	36.7 | 37.6

From the simulations, it was very difficult to use the VAD as a reactive device to control sound pressure over a broad bandwidth. The effect of the VAD was to reduce the amplitude of the in-phase panel/VAD modes by mass loading the panel modes. However, it also introduced an out-of-phase mode which boosted the sound transmission at high frequencies. In between the resonance frequencies of the two lowest order panel/VAD modes was a strong anti-resonance arising from the uncoupled VAD mode.

The baseline VAD designs were found to be effective at significantly reducing the sound transmission in the 50Hz to 200Hz band; however, the 50Hz to 400Hz band often experienced an increase in overall levels because of the effect of the VAD/panel out-of-phase mode.

The optimal VAD design used the TMD as a highly reactive device with an uncoupled resonance frequency just below the upper bound of the frequency band of interest. The optimal diaphragm configuration was highly lossy to reduce the modal amplitude of a single acoustic mode. Local flexure of the panel reduced the effectiveness of the VAD's and alternative attachment techniques were investigated to reduce such flexure, with a resulting improvement in performance as can be seen in the above table.

It should be noted that in almost all the cases considered, the equivalent mass (achieved by simply smearing the VAD mass over the flexible panel), provided the optimal passive control over the larger bandwidth. This is not surprising, since the VAD introduces another higher order mode which boosts high frequency transmission over the empty structure. The only benefit from the VAD (apart from the mass loading of the primary mode) is the anti-resonance (at the uncoupled VAD natural frequency). For the VAD to come close to canceling the unwanted gains of the higher order out-of-phase mode, the frequency of the anti-resonance must lie close to the upper bound of the frequency band of interest.

Contents

1   Introduction

The original objective of stage 1 of the project was to determine the optimal mass, stiffness and damping characteristics for passive noise control devices attached to the structure of a launch vehicle fairing to achieve a maximum reduction in interior noise levels for a specified added mass. However, during the processing of the original proposal, Dr Steve Griffin (the Air Force Technical monitor for the project), made considerable conceptual advances in similar work and based on this work and his request, it was decided to alter the objective slightly to, "the analytical development of an optimally tuned acoustic/vibration absorber that could be used to reduce interior noise levels by simultaneously controlling both the interior modal response and the enclosing structural modal response". Such an absorber consists of an acoustic absorber and a vibration absorber in the one device. This is realised in practice using a loudspeaker, which has an enclosed rear side and its front side exposed. The loudspeaker diaphragm and backing cavity act as an acoustic tuned absorber, while attaching the entire device to the structure using spring connectors provides the vibration absorber device.

The first stage of the project is to optimise the design of the entire device to minimise the noise transmitted into an experimental cylinder through an end cap on which the device is to be mounted. A considerable amount of experimental work had already been done by Dr Griffin's group at Kirtland Air Force Base prior to the beginning of the current project. Thus the first step in the optimal design process is to develop a numerical model of the experimental arrangement and compare the predicted results with those actually measured by Dr Griffin's team. The next step is to optimise the various parameters such as mass of the speaker diaphragm, volume of the speaker backing cavity, damping of the speaker diaphragm and backing cavity, diameter and length of a port in the speaker backing cavity and mass of the speaker and its enclosure to provide a maximum amount of interior noise reduction in the frequency ranges 50Hz-200Hz and 50Hz to 400Hz.

The preliminary report[1] concerned the development of the numerical model of the experimental arrangement used by Dr Griffin and the use of the model to investigate the effects of varying the parameters described above. This report, the final for the current contract, is concerned with the development and testing of a more efficient modal coupling procedure that can be used to analyse the effectiveness of a complex device mounted on a complex enclosure.

For Stage 2 of the project the current approach will be applied to the analysis of a more realistic composite cylinder (3m diameter and 4m tall) that Dr Griffin is planning to test at Boeing.

2   Background Theory

Prior to evaluating the effectiveness of the noise control system, it is first necessary to predict the response of the physical system (coupled structural/acoustic) to some excitation. This requires that either an analytical, numerical or experimental model of the vibro-acoustic system be developed, which then allows the calculation of the interior sound field generated by structural or acoustic sources.

This section develops a generalised numerical framework for the investigation of any arbitrarily shaped structure radiating periodic sound into a contiguous cavity. The model permits the use of both passive and active acoustic devices (both internal and external) as well as passive and active structural devices and allows for the investigation of a variety of passive and active feedforward control strategies.

There are many approaches available for solving the response of a coupled vibro-acoustic system. It was decided to use a combination of two approaches that have been successful in the past, namely *Modal Coupling Analysis* and *Finite Element Analysis*. The modal coupling approach developed by Lyon and Maidanik[2], Fahy[3], Pope[4] and Dowell et al.[5] and elegantly summarised by Fahy[6] provides a method for expressing the vibro-acoustic system in terms of the uncoupled modes of the fluid and the structure.

A finite element approach was chosen as the method to derive the modal models for two reasons: it does not suffer from the restriction that analytical models do, in that it allows objects of arbitrary geometry to be modelled; and suitable commercial FE code was available.

The modelling technique developed here has been numerically verified in Appendix A for the case of sound transmission through a cylindrical structure into a contiguous cavity. This system will also form the basis for the numerical study on the effects of passive reactive devices on sound transmission into cavities.

2.1 Modal Interaction Model

Much of the work detailed in the following chapter is not new (as is indicated by the references throughout). The analytical models of the system response were formulated by using the modal coupling theory of Pope[4] and Fahy[6].
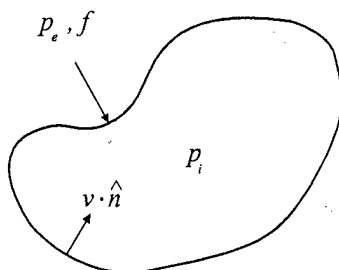
Figure 1: Arbitrary vibrating structure radiating into a contiguous cavity.

2.1.1 Uncoupled Response

In the following section a direct and concise derivation of the acoustic pressure of a cavity due to the motion of the bounding structure is given. The acoustic pressure is derived in terms of the normal modes of the *rigid-walled* cavity. The equations of motion of the structure are derived in terms of the *in vacuo* structural normal modes. Finally, the complete coupled fluid-structural equations of motion are obtained. Positive harmonic time dependence of the form $e^{j\omega t}$ is assumed for the analysis but has been omitted for the sake of brevity.

2.1.1.1 Rigid-Walled Acoustic Response Referring to Figure 1, it can be shown that in the absence of sources in the fluid, the acoustic pressure, p, subject to rigid-walled boundary conditions ($\partial p/\partial \hat{n} = 0$), satisfies the homogeneous wave equation[6]

$$\nabla^2 p - \frac{1}{c_0^2}\frac{\partial^2 p}{\partial t^2} = 0 \tag{1}$$

where c_0 is the speed of sound in air. The modal solution to Equation (1) at some point in the cavity, $\vec{r}$, is given by[7]

$$p(\vec{r}) = \sum_{l=1}^{\infty} p_l \phi_l(\vec{r}) \tag{2}$$

where p_l is the complex amplitude of the lth acoustic pressure mode defined by the mode shape function ϕ_l and natural frequency ω_l. For a monopole with volume velocity, q_c, operating in the cavity, it can be shown that the sound pressure at any point $\vec{r}$ in the enclosure is[4]

$$p(\vec{r}) = j\rho_0 \omega q_c G_a(\vec{r}_c \,|\, \vec{r}) \tag{3}$$

where ρ_0 is the density of the air, ω is the frequency of interest and $G_a(\vec{r}_c \,|\, \vec{r})$ is the Green's function of the acoustic space given by

$$G_a(\vec{r}_c \,|\, \vec{r}) = \sum_{l=1}^{\infty} \frac{\phi_l(\vec{r}_c)\phi_l(\vec{r})}{\Lambda_l Z_l} \tag{4}$$

where Λ_l is the modal volume of the lth cavity mode, defined as the volume integration of the square of the mode shape function, ie

$$\Lambda_l = \int_V \phi_l^2(\vec{r}) dV(\vec{r}) \tag{5}$$

where V is the volume of the cavity. Z_l is the rigid-walled acoustic input impedance of the lth cavity mode given by

$$Z_l = (k_l^2 + j\eta_{a_l} k_l k - k^2) \tag{6}$$

where k is the wavenumber of the sound in the cavity, k_l is the lth eigenvalue of the cavity, η_{a_l} is the viscous modal loss factor of the lth acoustic mode which is equal to twice the critical damping ratio, ξ_{a_l}, of the lth cavity mode.

The pressure in the cavity from the operation of L_a acoustic sources is given by the linear superposition of the pressure due to each source given by Equation (3)[8]

$$p(\vec{r}) = \sum_{i=1}^{L_a} j\rho_0 \omega q_{c,i} G_a(\vec{r}_{c,i} \,|\, \vec{r}) \tag{7}$$

where $q_{c,i}$ is the volume velocity of the ith acoustic source located at a position $\vec{r}_{c,i}$ in the acoustic space.

In practice the Green's function (Equation (4)) is not evaluated over all modes but rather over a subset of modes, say n_a acoustic modes. This is necessary for numerical modelling as it keeps the size of the matrices manageable. For the numerical analysis Equation (7) can be rewritten in matrix form in terms of the modal pressure amplitudes, $\mathbf{p}$, and the generalised volume velocity, $\mathbf{Q}$, ie

$$p(\vec{r}) = \phi^T(\vec{r})\mathbf{p} = \phi^T(\vec{r}) \left[j\rho_0 \omega \Lambda^{-1} \cdot \mathbf{Z}_l^{-1} \mathbf{Q} \right] \tag{8}$$

where $\phi(\vec{r})$ is the (n_a x 1) column vector of the n_a acoustic modes evaluated at $\vec{r}$, $\mathbf{p}$ is the (n_a x 1) column vector of pressure modal amplitudes, Λ is the (n_a x n_a) diagonal modal volume matrix, the diagonal elements of which are given by Equation (5), $\mathbf{Z}_l$ is the (n_a x n_a) diagonal rigid-walled acoustic input impedance matrix, the diagonal elements of which are given by

Equation (6) and $\mathbf{Q}$ is the (n_a x 1) generalised volume velocity vector, the lth element of which is given by $Q_l = \int_V q(\vec{r})\phi_l(\vec{r})dV$.

The $\cdot$ in Equation (8) indicates the element by element product of the two arrays[9]. For example, given two (m x n) matrices $\mathbf{A}$ and $\mathbf{B}$, then

$$\mathbf{A} \cdot \mathbf{B} = \begin{bmatrix} a_{11}b_{11} & a_{12}b_{12} & \cdots & a_{1n}b_{1n} \\ a_{21}b_{21} & a_{22}b_{22} & \cdots & a_{2n}b_{2n} \\ \vdots & \vdots & \ddots & \vdots \\ a_{m1}b_{m1} & a_{m1}b_{m1} & \cdots & a_{mn}b_{mn} \end{bmatrix} \tag{9}$$

It should be noted for the case of the matrix $\mathbf{A}$ is diagonal then $\mathbf{A} \cdot \mathbf{B} = \mathbf{AB}$. This approach was used to increase the speed of the simulations. For L discrete sources the total generalised volume velocity vector of the discrete modal system is,

$$\mathbf{Q} = \Phi_l \mathbf{q}^{\mathsf{T}} \tag{10}$$

where Φ_l is the (n_a x L_a) matrix of acoustic mode shape functions evaluated at the L source locations and $\mathbf{q}$ is the (1 x L_a) row vector of acoustic source strengths.

2.1.1.2 *In-vacuo* Structural Response

An expression for the structural velocity at some point on the structure, $\vec{x}$, can be derived in terms of its *in vacuo* modes as given by[8]

$$v(\vec{x}) = \sum_{i=1}^{\infty} v_i \psi_i(\vec{x}) \tag{11}$$

where v_i is the complex amplitude of the ith structural mode defined by the mode shape function ψ_i and natural frequency ω_i.

For a point force of strength, f_c, operating normal to the structure, it can be shown that the velocity at any point $\vec{x}$ on the structure is[4]

$$v(\vec{x}) = j\omega f_c \delta(\vec{x} - \vec{x}_c) G_s(\vec{x}_c | \vec{x}) \tag{12}$$

where $G_s(\vec{x}_c | \vec{x})$ is the Green's function of the structure given by

$$G_s(\vec{x}_c | \vec{x}) = \sum_{i=1}^{\infty} \frac{\psi_i(\vec{x}_c)\psi_i(\vec{x})}{M_i Z_i} \tag{13}$$

and where M_i and Z_i are the modal mass and the *in vacuo* structural input impedance of the ith mode respectively, given by

$$M_i = \int_S m(\vec{x})\psi_i^2(\vec{x})dA(\vec{x}) \tag{14}$$

$$Z_i = (\omega_i^2 + j\eta_{s_i}\omega_i^2 - \omega^2) \tag{15}$$

in which $m(\vec{x})$ is the surface density of the structure and η_{s_i} is the modal loss factor of the ith structural mode.

The velocity on the structure from the operation of L_s forces is given by the linear superposition of the velocity due to each source given by Equation (12)[8]

$$v(\vec{x}) = \sum_{i=1}^{L_s} j\omega f_{c,i} \delta(\vec{x} - \vec{x}_{c,i}) G_s(\vec{x}_{c,i} | \vec{x}) \tag{16}$$

where $f_{c,i}$ is the ith force located at a position $\vec{x}_{c,i}$ in the structure.

As was the case with the acoustic Green's function, the structural Green's function (Equation 4) is also truncated to a subset of modes, say n_s structural modes. Equation (16) can be rewritten in matrix form in terms of the modal velocity amplitudes, $\mathbf{v}$, and the modal generalised force, $\mathbf{F}$, as

$$v(\vec{x}) = \psi^T(\vec{x})\mathbf{v} = \psi^T(\vec{x}) \left[j\omega\mathbf{M}^{-1} \cdot \mathbf{Z}^{-1}\mathbf{F} \right] \tag{17}$$

where $\psi(\vec{x})$ is the (n_s x 1) column vector of the n_s structural modes evaluated at $\vec{x}$, $\mathbf{v}$ is the (n_s x 1) column vector of velocity modal amplitudes, $\mathbf{M}$ is the (n_s x n_s) diagonal modal mass matrix, the diagonal elements of which are given by Equation (14), $\mathbf{Z}$ is the (n_s x n_s) diagonal *in vacuo* structural input impedance matrix, the diagonal elements of which are given by Equation (15) and $\mathbf{F}$ is the (n_s x 1) generalised force column vector, the ith element of which is given by $F_i = \int_s f(\vec{x})\psi_i(\vec{x})dS$.

For L_s discrete forces the total generalised force vector of the discrete modal system is,

$$\mathbf{F} = \Psi_i \mathbf{f}^T \tag{18}$$

where Ψ_i is the (n_s x L_s) matrix of structural mode shape functions evaluated at the L_s force locations and $\mathbf{f}$ is the (1 x L_s) row vector of discrete complex forces.

2.1.2 Coupled Response

Having derived the uncoupled modal models it is necessary to couple them using modal coupling theory. The fluid pressure on the surface of the structure is the agent by which the fluid influences structural motion, and the normal surface velocity of the structure is the agent by which the structure influences the fluid[6].

The governing equation for the coupled vibro-acoustic system is the inhomogeneous wave equation

$$\nabla^2\Phi - \frac{1}{c_0^2}\frac{\partial^2\Phi}{\partial t^2} = q \tag{19}$$

where Φ is the acoustic potential function and is related to the acoustic pressure and fluid particle velocity by the following

$$p = -\rho_0\frac{\partial\Phi}{\partial t} \tag{20}$$

$$v = \nabla\Phi \tag{21}$$

Therefore, if the boundaries of the cavity are rigid then $\partial\Phi/\partial\hat{n} = 0$, where $\hat{n}$ is the normal to the boundary surface. The boundary condition over a flexible structure is determined by continuity of the normal air particle velocity and the normal structure velocity on the surface (positive normal outwards), ie $\partial\Phi/\partial\hat{n} = \partial w/\partial t$, where w is the structural displacement normal to the surface. It can be shown that the coupled modal equations of motion for the structure and the cavity in terms of the w and Φ are given by[6]

$$\ddot{w}_i + \omega_i^2 w_i = -\frac{\rho_0 S}{M_i}\sum_{l=1}^{\infty}\dot{\Phi}_l B_{l,i} + \frac{F_i}{M_i} \tag{22}$$

$$\ddot{\Phi}_l + \omega_l^2\Phi_l = \frac{c_0^2 S}{\Lambda_l}\sum_{i=1}^{\infty}\dot{w}_i B_{l,i} - \frac{c_0^2 Q_l}{\Lambda_l} \tag{23}$$

where Φ_l is the potential of the lth acoustic mode, Q_l and Λ_l are the generalised volume velocity and modal volume of the lth acoustic mode, w_i is the modal displacement of the ith structural mode (positive normal outwards), F_i and M_i are the generalised force and modal mass of the ith structural mode. $B_{l,i}$ is the non-dimensional coupling coefficient between the lth acoustic mode and the ith structural mode, defined as[4]

$$B_{l,i} = \frac{1}{S} \int_S \phi_l(\vec{r}) \psi_i(\vec{r}) dA(\vec{r}) \tag{24}$$

It is possible to rearrange Equations (22) and (23) in terms of the modal amplitudes of the structural velocity and cavity pressure. Solving Equation (23) for arbitrary frequency ω and using the expression $\ddot{\Phi}_l = -\omega^2 \Phi_l$ gives

$$\Phi_l = \frac{c_0^2}{\Lambda_l(\omega_l^2 - \omega^2)} \left[S \sum_{i=1} v_i B_{l,i} - Q_l \right] \tag{25}$$

Adding the *ad hoc* damping terms for the cavity, $j\eta_{a_p}\omega_p\omega$, to Equation (25) and using $p = -\rho_0 \frac{\partial \Phi}{\partial t} = -j\rho_0\omega\Phi$ an expression for the modal pressure in the cavity resulting from both the structure and interior acoustic sources is given by

$$p_l = \frac{j\rho_0 c_0^2 \omega}{\Lambda_l(\omega_l^2 + j\eta_{a_l}\omega_l\omega - \omega^2)} \left[-S \sum_{i=1} v_i B_{l,i} + Q_l \right] \tag{26}$$

and rewriting in terms of the acoustic wavenumber,

$$p_l = \frac{j\rho_0\omega}{\Lambda_l(k_l^2 + j\eta_{a_l}k_lk - k^2)} \left[-S \sum_{i=1} v_i B_{l,i} + Q_l \right] \tag{27}$$

Likewise, solving Equation (22) for arbitrary frequency ω and using the expressions $\ddot{w}_i = -\omega^2 w_i$ and $\dot{\Phi}_l = -p_l/\rho_0$ gives

$$w_i = \frac{1}{M_i(\omega_i^2 - \omega^2)} \left[S \sum_{l=1} p_l B_{l,i} + F_i \right] \tag{28}$$

Adding the *ad hoc* damping terms for the structure, $j\eta_{s_i}\omega_i^2$, to Equation (28) and using $v_i = \dot{w}_i = j\omega w_i$ an expression for the modal velocity of the structure resulting from both interior acoustic and structural forces is given by

$$v_i = \frac{j\omega}{M_i(\omega_i^2 + j\eta_{s_i}\omega_i^2 - \omega^2)} \left[S \sum_{l=1} p_l B_{l,i} + F_i \right] \tag{29}$$

2.1.2.1 Structure to acoustic interior transfer function, $\mathbf{Z}_a$ The modal pressure amplitudes of the cavity as a result of the vibration of the structure can be obtained from Equation (27)

$$\mathbf{p} = \mathbf{Z}_a \mathbf{v} \tag{30}$$

where $\mathbf{Z}_a$ is the (n_a x n_s) structural to acoustic modal internal radiation transfer function matrix, the terms of which are

$$Z_a(l,i) = -\frac{j\rho_0 S\omega}{\Lambda_l(k_l^2 + j\eta_{a_l}k_lk - k^2)} B_{l,i} \tag{31}$$

Although derived independently through a potential formulation, Equation (32) is identical to that given by Snyder and Hansen[8] apart from the sign of the expression. Therefore, for a positive normal directed into the cavity, $\mathbf{Z}_a$ is given by

$$Z_a(l,i) = \frac{j\rho_0 S\omega}{\Lambda_l(k_l^2 + j\eta_{a_l}k_l k - k^2)}B_{l,i} \tag{32}$$

2.1.2.2 Interior acoustic to structure transfer function, $\mathbf{Z}_b$

Rewriting Equation (29) in matrix form the modal velocity amplitudes of the structure arising from the acoustic pressure are given by

$$\mathbf{v} = \mathbf{Z}_b\mathbf{p} \tag{33}$$

where $\mathbf{Z}_b$ is the ($n_s \times n_a$) acoustic to structural modal internal radiation transfer function, the terms of which are

$$Z_b(l,i) = \frac{jS\omega}{M_i Z_i}B_{l,i} \tag{34}$$

For a positive normal directed inwards $\mathbf{Z}_b$ is given by

$$Z_b(l,i) = -\frac{jS\omega}{M_i Z_i}B_{l,i} \tag{35}$$

2.1.2.3 Solution of coupled system of equations

Acoustic sources   Consider the forced response of the system due to acoustic sources only. The cavity response is given by Equation (27). The closed-form solution for the cavity response with a positive normal directed outwards is obtained with the substitution into Equation (29) of Equation (27) for the velocity amplitudes and neglecting the force term,

$$p_r = \frac{j\rho_0\omega}{\Lambda_r(k_r^2 + j\eta_{a_r}k_r k - k^2)}\left[-S\sum_{i=1}^{\infty}\frac{j\omega}{M_i Z_i}\left[S\sum_{l=1}^{\infty}p_l B_{l,i}\right]B_{r,i} + Q_r\right] \tag{36}$$

Rearranging gives,

$$\frac{-j\Lambda_r(k_r^2 + j\eta_{a_r}k_r k - k^2)}{\rho_0\omega}p_r = j\omega S^2\sum_{i=1}^{\infty}\sum_{l=1}^{\infty}\frac{B_{l,i}B_{r,i}}{M_i Z_i}p_l + Q_r \tag{37}$$

For a positive normal directed inwards, the above expression becomes,

$$\frac{-j\Lambda_r(k_r^2 + j\eta_{a_r}k_r k - k^2)}{\rho_0\omega}p_r = -j\omega S^2\sum_{i=1}^{\infty}\sum_{l=1}^{\infty}\frac{B_{l,i}B_{r,i}}{M_i Z_i}p_l + Q_r \tag{38}$$

If the infinite sums over l and i are truncated to n_a acoustic modes and n_s structural modes, respectively, the response of the cavity to the finite number of monopole sources can be written in matrix form as,

$$\mathbf{p} = \mathbf{Z}_q^{-1}\mathbf{Q} \tag{39}$$

where $\mathbf{p}$ is the ($n_a \times 1$) vector of acoustic pressure participation factors (each element of which represents the modal pressure amplitude of a particular acoustic mode), $\mathbf{Q}$ is the total ($n_a \times 1$) generalised volume velocity vector (each element of which represents the relative contribution

of the acoustic sources to a particular mode) and $\mathbf{Z}_q$ is the (n_a x n_a) acoustic modal input impedance matrix for a positive normal directed inwards, the terms of which are,

$$Z_q(u,u) \;=\; j\omega S^2 \sum_{i=1}^{n_s} \frac{B_{u,i}B_{u,i}}{M_i Z_i} - \frac{j\Lambda_u(k_u^2 + j\eta_{a_u}k_u k - k^2)}{\rho_0 \omega}, \text{diagonal terms}$$

$$Z_q(u,v) \;=\; j\omega S^2 \sum_{i=1}^{n_s} \frac{B_{u,i}B_{v,i}}{M_i Z_i}, \text{off} - \text{diagonal terms} \tag{40}$$

where u and v refer to the uth and v^{th} acoustic modes, $Z_q(u,v)$ represents the pressure response of mode v to a unit response of mode u. It should be noted that the inverse of the second term for the diagonal expression is simply the volume velocity to pressure impedance matrix for rigid walled conditions.

The term $j\omega S^2 \sum_{i=1}^{n_s} \frac{B_{u,i}B_{v,i}}{M_i Z_i}$ is known as the gyrostatic coupling term. It was neglected by Snyder and Hansen[8], although they refer to the work of Pan[10] which provides details on how to include the effects of coupling in their set of equations. It should be noted that for some weakly coupled structural acoustic systems it is possible to neglect the structural/acoustic interaction when predicting the sound pressure field in the enclosure under operation of the acoustic sources alone. However, at the structural resonances, neglecting this interaction in realistic systems may result in some discrepancy between the theoretical and experimental results[11,12] and without this term structural-acoustic reciprocity does not hold.

Structural sources   Consider the forced response of the system due to structural forces only. The structural response is given by Equation (29). The solution for the structural response is obtained by substituting Equation (27) for the pressure amplitudes into Equation (29) and neglecting the volume velocity term,

$$v_r = \frac{j\omega}{M_r Z_r} \left[-S \sum_{l=1}^{\infty} \frac{j\rho_0\omega}{\Lambda_l(k_l^2 + j\eta_{a_l}k_l k - k^2)} \left[S \sum_{i=1}^{\infty} v_i B_{l,i} \right] B_{l,r} + F_r \right] \tag{41}$$

Rearranging,

$$\frac{-jM_r Z_r}{\omega} v_r = -j\omega\rho_0 S^2 \sum_{i=1}^{\infty} \sum_{l=1}^{\infty} \frac{B_{l,i}B_{l,r}}{\Lambda_l(k_l^2 + j\eta_{a_l}k_l k - k^2)} v_i + F_r \tag{42}$$

If the infinite sums over l and i are truncated to n_a acoustic modes and n_s structural modes, respectively, the response of the structure to the finite number of forces can be written in matrix form,

$$\mathbf{v} = \mathbf{Z}_I^{-1}\mathbf{F} \tag{43}$$

where $\mathbf{v}$ is the (n_s x 1) vector of structural modal velocity participation factors, $\mathbf{F}$ is the total generalised force and $\mathbf{Z}_I$ is the (n_s x n_s) structural modal input impedance matrix, the terms of which are,

$$Z_I(u,u) = j\omega\rho_0 S^2 \sum_{l=1}^{n_a} \frac{B_{l,u}B_{l,u}}{\Lambda_l(k_l^2 + j\eta_{a_l}k_l k - k^2)} - \frac{jM_u Z_u}{\omega}, \text{diagonal terms}$$

$$Z_I(u,v) = j\omega\rho_0 S^2 \sum_{l=1}^{n_a} \frac{B_{l,u}B_{l,v}}{\Lambda_l(k_l^2 + j\eta_{a_l}k_l k - k^2)}, \text{off} - \text{diagonal terms} \tag{44}$$

where u and v refer to the uth and v^{th} structural modes, $Z_I(u,v)$ represents the structure response of mode v to a unit response of mode u. It should be noted that the inverse of the second term for the diagonal expression is simply the force to velocity impedance matrix for the *in vacuo* structure. This expression is identical to that derived by Snyder and Hansen[8].

2.1.2.4 Generalised expression for coupled response   Using Equations (39), (30) and (43) the modal pressure amplitudes arising from both monopole volume velocity sources and structural point forces are given by

$$\mathbf{p} = \mathbf{Z}_q^{-1}\mathbf{Q} + \mathbf{Z}_a\mathbf{Z}_I^{-1}\mathbf{F} \qquad (45)$$

The pressure at a point can be obtained by substitution of Equation (45) into Equation (2). Using Equations (39), (33) and (43) the modal structural velocities arising from both monopole volume velocity sources and structural point forces are given by

$$\mathbf{v} = \mathbf{Z}_b\mathbf{Z}_q^{-1}\mathbf{Q} + \mathbf{Z}_I^{-1}\mathbf{F} \qquad (46)$$

The velocity at a point on the structure can be obtained by substitution of Equation (46) into Equation (11).

2.1.3 Limitations of the Modal Coupling Approach

It should be noted that since the acoustic modes are for a rigid walled enclosure, then the solution for the acoustic pressure based on the finite modal expansion, though accurate in the interior of the cavity, does not converge to the boundary normal velocity. This mathematical condition associated with finite summations is referred to as Gibb's phenomenon. Since the rigid walled acoustic modes satisfy the Neumann boundary condition, the velocity predicted at the boundary is zero and this inaccuracy in the velocity field can be substantial in the vicinity of vibrating boundaries[6,13]. Therefore, this technique is inappropriate for investigating the impedance conditions, sound intensity or energy density at the vibrating boundaries of the enclosure.

The error in the velocity (pressure gradient) is a function of the proximity to the boundary and the number of acoustic modes used in the expansion, or more specifically the acoustic wavelength at the largest acoustic mode. Jayachandran et al.[13] have investigated the effects of the inaccuracies at the boundaries of a coupled vibro-acoustic system and found that the inaccuracies do not affect the control prediction when minimising the acoustic potential energy.

3 The Numerical Model and Verification

In the preliminary report by Hansen et al.[1], it was shown that the modal coupling theory (as describe in Section 2) produced similar results for a rectangular cavity coupled to a flexible rectangular plate when compared to the results obtained using a fully coupled FE solution within ANSYS. The verification has been extended here to the cylindrical structure seen in Figures 2 and 3. The results of the validation of the numerical technique (including FEA, BEA and modal coupling) can be found in the Appendices.

The material presented below is aimed specifically at verifying that the numerical model accurately emulates the experimental test rig and that the results from the model and the rig compare favorably.

3.1 The experimental rig

The numerical simulations used a Finite Element model based on the experimental apparatus shown in Figure 2. One end of the cylinder is closed with a flexible aluminum panel, while the other end is closed with rigid plywood. Photographs of the apparatus are shown in Figure 3. The dimensions and material properties of the rig are detailed in Table 1.
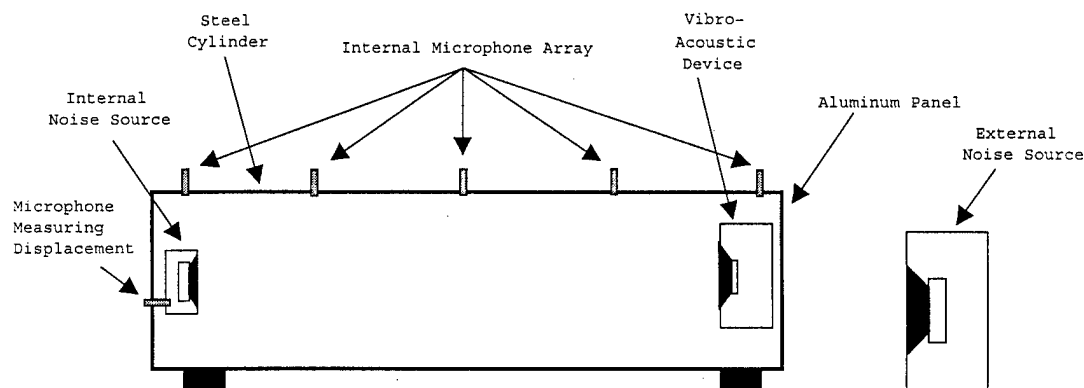

Figure 2: Experimental Setup

3.2 Cavity

From the experimental transfer functions taken between a microphone measuring the volume velocity of a loudspeaker mounted in the cylinder and an internal microphone (see Figure 4, cavity), the resonance frequencies of the first two modes of the coupled cavity are approximately 79 Hz and 160 Hz.

Theoretically the natural frequencies of the longitudinal modes of the cavity (assuming rigid walls) are given by the following expression

$$f_{a_n} = \frac{c_0 n}{2l}$$

where c_0 is the speed of sound in the air, n is the order of the mode and l is the length of the cavity. For the parameters detailed in Table 1, the first 3 natural frequencies of the uncoupled cavity are given in Table 2. Comparing the measured resonance frequencies and the theoretical it can be seen that the coupling between the structure and the cavity is weak. If it were strong there would be a significant difference between the two sets of values.

The modal loss factor of the cavity, η_a, was determined by measuring the half power bandwidth (3dB bandwidth), Δf_{3dB}, from Figure 4 and using the following expression $\eta_a = \Delta f_{3dB}/f$. Using this expression the acoustic modal loss factor was estimated to be 3.5%.

3.2.1 Acoustic FEM

The acoustic FEM of the cylindrical cavity can be seen in Figure 5. The material properties used for the FE model are detailed in Table 1. There were 6183 nodes and 5616 brick elements. A modal analysis was conducted on the FE model and all modes below 800Hz were extracted, the first 9 of which are listed in Table 3. There were approximately 9 elements per wavelength at 400 Hz. This means that the natural frequencies of the calculated cavity modes are accurate
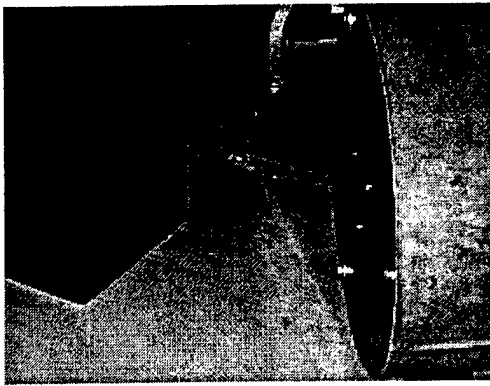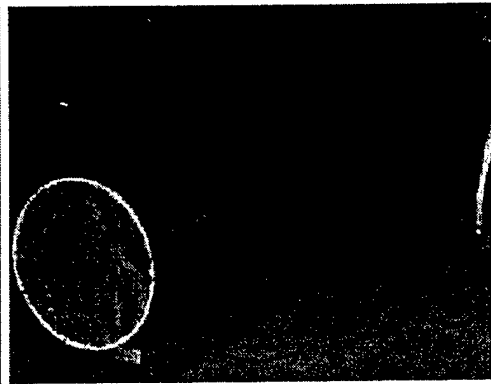
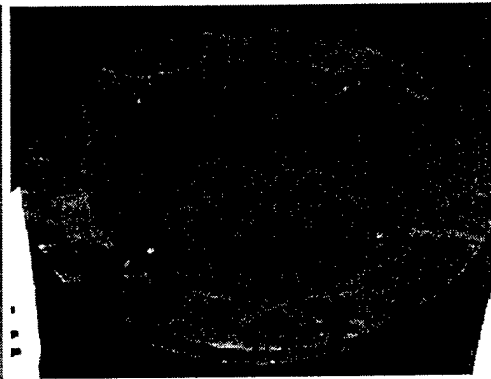(a) Aluminum plate   (b) Steel cylinder
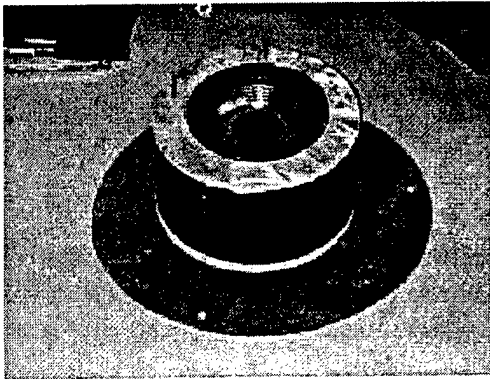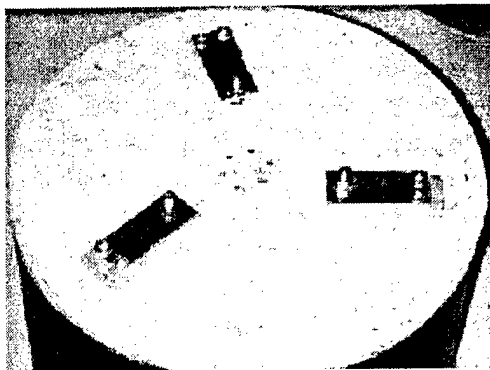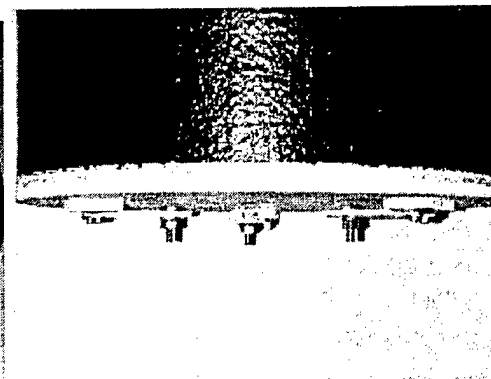

(c) Vibro-acoustic device   (d) Tuned mass damper

(e) VAD/TMD suspension   (f) Suspension close-up

Figure 3: Photographs of Experimental Setup

| Object	Parameter	Value
Cylinder (steel)	Overall length, l	2.142 m
	Outside diameter, d	0.514 m
	Wall thickness, t_s	6.35 mm
	Young's Modulus, E_s	207 GPa
	Density, ρ_s	7850 kg/m^3
	Poisson's Ratio, ν_s	0.3
Aluminum Plate	Outside diameter, d	0.514 m
	Thickness, t_{al}	3.376 mm
	Mass	1.854 kg
	Young's Modulus, E_{al}	70 GPa
	Density, ρ_{al}	2700 kg/m^3
	Poisson's Ratio, ν_{al}	0.3
	Structural Modal Loss Factor, η_s	2%
Plywood End-Cap	Outside diameter, d	0.514 m
	Thickness, t_{wood}	12.7 mm
	Young's Modulus, E_{wood}	10 GPa
	Density, ρ_{wood}	800 kg/m^3
	Poisson's Ratio, ν_{wood}	0.3
Vibro-Acoustic Device	Diameter	0.298 m
	Height	0.165 m
	Mass	2.077 kg
	Uncoupled frequency of TMD	135 Hz, 3% damping
VAD Diaphragm	Diameter	0.154 m
	Mass	26.5 g
	Volume of air behind diaphragm	9 l
	Uncoupled frequency in device	80 Hz, 10% damping
Equivalent Mass	3 Aluminum blocks	2.056 kg
Acoustic Space	Density, ρ_0	1.21 kg/m^3
	Speed of Sound, c_0	343 m/s
	Acoustic Modal Loss Factor, η_a	3.5%

Table 1: Physical parameters of the setup
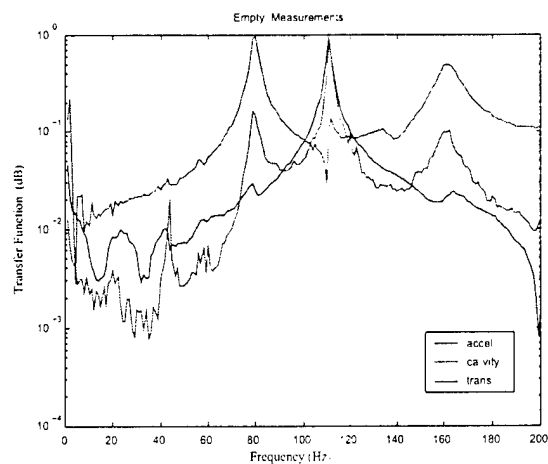
Figure 4: Measured transfer functions of the coupled system without the VAD: *accel* is the transfer function between a force applied to the panel and the velocity response on the panel, *cavity* is the transfer function between an internal acoustic source and an internal microphone, and *trans* is the transfer function between an external source and an internal microphone.

Mode	Frequency (Hz)
0	0
1	80
2	160

Table 2: Theoretical natural frequencies of the first 3 uncoupled longitudinal acoustic cavity modes

to at least 600 Hz. Some of the modes with natural frequencies higher than this (particularly the longitudinal modes) are artificially stiffened leading to higher natural frequencies than the theoretical. It should be noted however, that these higher order modes have little affect on the system response apart form their stiffness residues, the contribution from which at low frequencies is unaffected by small changes in the natural frequencies.
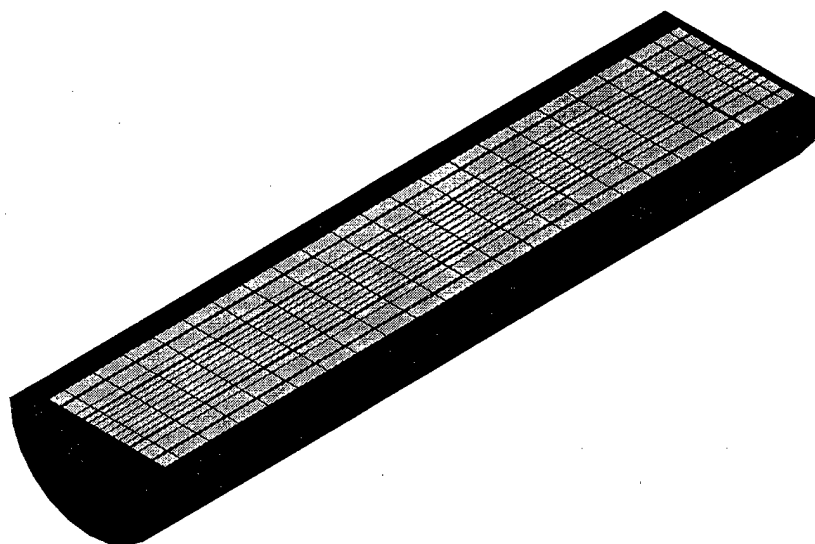

Figure 5: Section of finite element model of the cylindrical cavity.

3.3 Structure

The resonance frequency of the fundamental panel mode of the coupled aluminium end cap is approximately 110 Hz. This was determined from the experimental transfer functions (see Figure 4, accel) taken between a force transducer attached on the plate and an accelerometer on the plate.

Theoretically the natural frequency of the fundamental bending mode of the circular plate (assuming *in-vacuo*) is given by the following expression[14]

$$f_{al_{0,0}} = \frac{k}{2\pi a^2} \sqrt{\frac{D}{\rho_{al}}}$$

where k is a constant dependent on the boundary conditions, a is the radius of the plate, $D = E_{al} t_{al}^3 / (12(1 - v_{al}^2))$ is the flexural rigidity and ρ_{al} is the density of aluminium. For the parameters detailed in Table 1 the natural frequencies of the uncoupled fundamental panel mode for a simply supported and fully clamped boundary condition are given in Table 4. Comparing the measured and theoretical resonance frequency of the panel it can be seen that the boundary condition lies somewhere between simply supported and fully clamped.

The modal loss factor of the structure, η_s, was determined using the same technique as for the cavity. From Figure 4 the structural modal loss factor was estimated to be approximately 2%.

Mode	Uncoupled Frequency
	(Hz)
0	1E-05
1	80.3
2	160.7
3	241.3
4	322.2
5	396.3
6	396.3
7	403.5
8	404.4
9	404.4

Table 3: Calculated natural frequencies of the first 9 acoustic cavity modes.

Boundary Condition	Frequency (Hz)
Simply Supported	62.4
Fully Clamped	128.5

Table 4: Natural Frequency of the uncoupled fundamental panel mode for various edge boundary conditions.

3.3.1 Structure FEM

The FEM of the cylindrical structure can be seen in Figure 6. There were 1058 nodes and 1056 (shell and brick) elements. The material properties used for the FE model are detailed in Table 1. The aluminium end cap was originally assumed to be fixed directly to the steel cylinder. A modal analysis was conducted on the structural FE model and all modes below 800 Hz were extracted, the first 18 of which are listed in Table 5. It can be seen that the calculated and measured resonance frequencies of the fundamental panel mode (mode 1) differ significantly. In fact, the calculated resonance frequency of the panel mode is very close to that of a fully clamped circular panel. In order to bring the numerically calculated natural frequency of the panel mode (assuming essentially clamped boundary conditions) down to match that measured experimentally, the Young's modulus of the panel material was reduced to 75% of its original value. This technique was used rather than modifying the coupling boundary conditions at the interface between the panel and the cylindrical shell, because of the inherent difficulties of such an approach. The recalculated natural frequencies are also shown in Table 5.
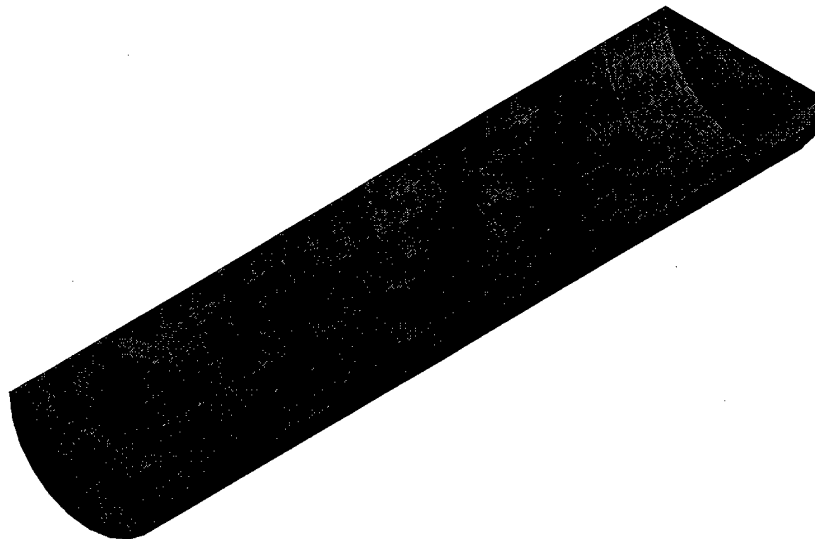

Figure 6: Finite element model of the cylindrical structure. The colours of the elements represents the element type; Red is the aluminium panel, Blue is the steel shell and Magenta is the plywood end-cap.

3.4 Coupled System

The forced response of the cavity for an internal acoustic source is shown in Figure 7. The results in the figure also illustrate the effect that the bulk compression mode has on the low frequency results. The different cases considered were; the standard modal volume of the bulk compression mode, a 10 times increase in the modal volume, a 100 times increase, and an infinite modal volume of the bulk compression mode.

Although the drive point and response point for the experiment and numerical simulation are not necessarily the same in Figures 4(cavity) and 7 respectively, they do show the same trends. However, the results below a marked difference below 50 Hz. This may be because of poor transducer response used for the measurements, or it may be due to a real phenomenon

Mode	Frequency (Hz)	
	Uncoupled	Uncoupled*
1	58.1	57.0
2	126.2	**111.3**
3	**128.3**	125.6
4	142.1	141.8
5	198.5	198.6
6	209.5	209.4
7	251.4	**232.9**
8	**268.4**	**232.9**
9	**268.4**	249.8
10	280.6	278.8
11	286.5	286.0
12	294.3	289.9
13	317.3	317.1
14	361.7	358.9
15	375.2	375.2
16	375.4	375.4
17	407.4	383.6
18	407.4	383.6

Table 5: Calculated natural frequencies of the first 9 structural modes. Panel modes are shown in bold type face. * Modified panel stiffness.

such leakage from the cylinder. In any case, the VAD was optimised from 50 Hz upwards so it has little bearing on the band averaged results.
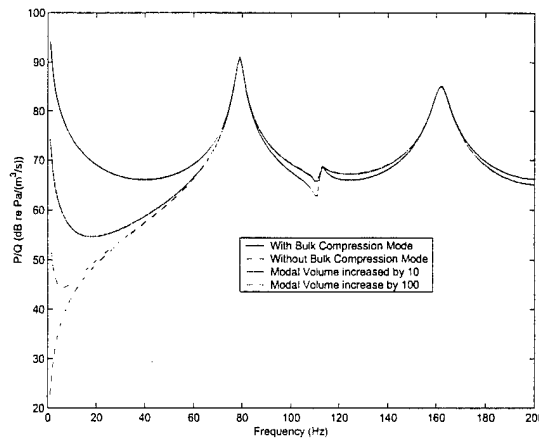
Figure 7: Predicted acoustic transfer function of the coupled system without the VAD.

The forced response of the structure due to a point force was calculated and is shown in Figure 8. Again, although the drive point and response point for the experiment and numerical simulation are not necessarily the same in Figures 4(accel) and 8 respectively, they do show the same trends.
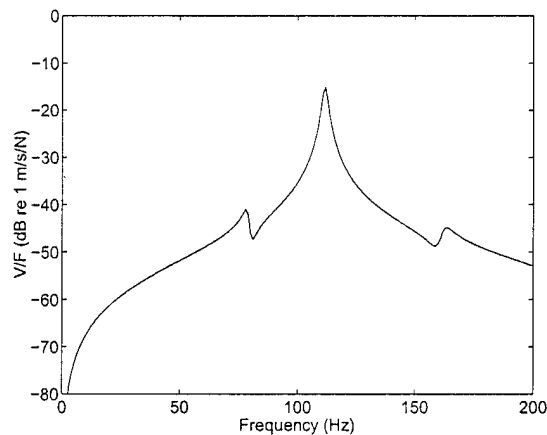
Figure 8: Predicted structural transfer function of the coupled system without the VAD.

The transfer functions of the coupled system were calculated between an external acoustic input and the pressure response response at a single location. These are shown in Figure 9. These compare favorably to the measured results shown in Figure 4 (trans).

From the forced response simulations for the empty cylinder, the numerical model appears to be providing accurate results.

3.5 Vibro-Acoustic Device

The effect of the vibro-acoustic device on the system dynamics can be seen by comparing the experimental results without the VAD in Figure 4 with those for the VAD in Figure 10.
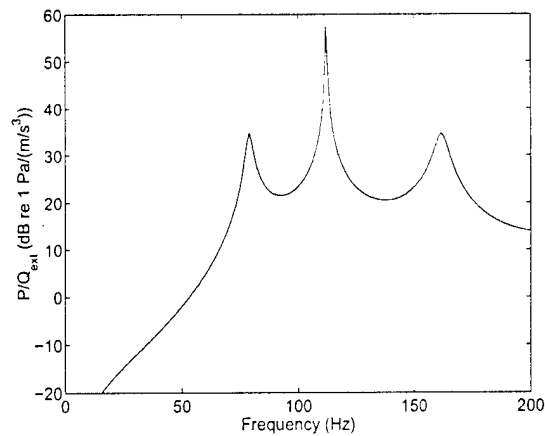
Figure 9: Predicted acoustic transfer functions of the coupled system.

The effect of the VAD on the space averaged SPL inside the cavity is also shown in Figure 11. The figure shows a transfer function from voltage in to the disturbance speaker amplifier to the spatially averaged pressure at several microphones for four separate cases, namely: Empty cylinder, Equivalent mass, Tuned mass damper and the Vibro acoustic device.

The empty case has no vibro-acoustic device. The equivalent mass has aluminum bricks whose mass adds up to the same total mass as the device attached to the plate at the points that the device attaches. Since the masses were attached directly to the panel rotational inertia was not present. The TMD (tuned mass damper) case is the vibro-acoustic device with a stiff Plexiglas panel in place of the diaphragm. Finally, VAD stands for the vibro-acoustic device results. Taking the sum the squares for each result over the frequency band and then taking the square root of that sum, the overall band performance is calculated. Table 6 gives the reduction in the overall space averaged sound pressure levels.
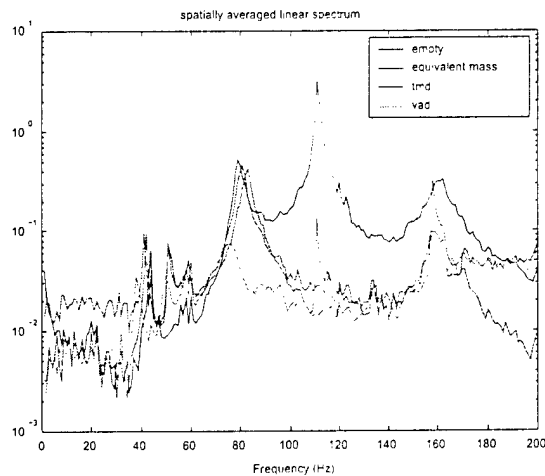

Figure 10: Measured acoustic transfer functions of the coupled system with the VAD.
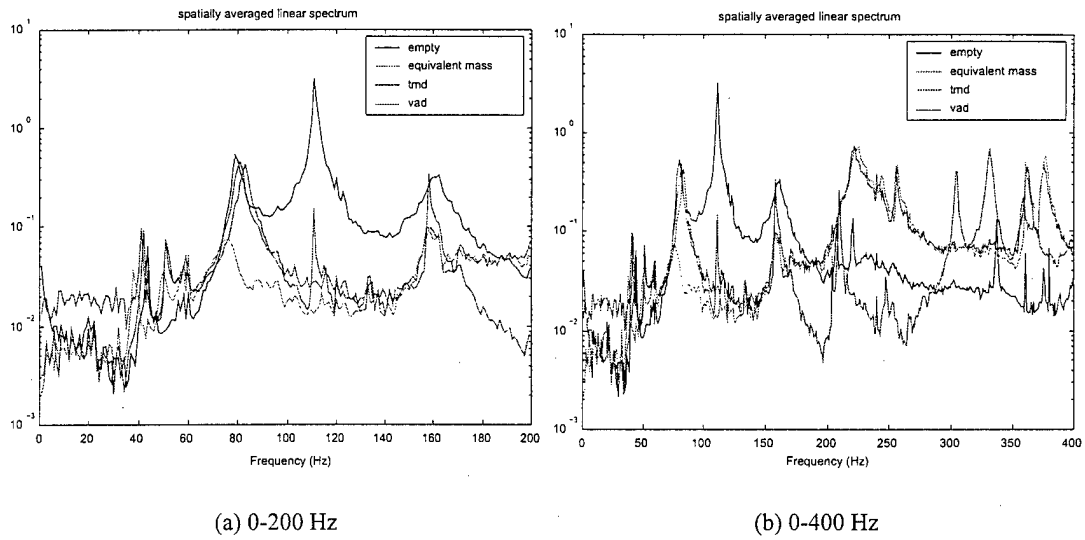
(a) 0-200 Hz   (b) 0-400 Hz

Figure 11: Spatially averaged SPL's of the coupled system with the VAD.

Test Case	Overall SPL Reduction (dB)
	Measured
Empty	0.0
Equivalent Mass	2.5
TMD	3.8
VAD	4.3

Table 6: Overall reduction in space averaged SPL (0-200Hz).

3.5.1 FEM of the VAD

The cross section of the FEM for the complete cylindrical structure and VAD can be seen in Figure 12. The material properties used for the FE model are detailed in Table 1.

Since the VAD for this particular configuration occupies a considerable volume of the cavity, it was necessary to calculate the response of the shell interior with the volume occupied by the VAD absent. It may be seen that for smaller more discrete VAD's it could be assumed that the volume occupied by the units is small relative to the overall cavity volume. If this is the case, then the effect of the VAD's volume could be ignored. This would mean that the same acoustic model could be used each time. This is the likely approach that will be used for Stage 2 of the project when the position as well as the dynamics of the VAD is to be optimised.

Two acoustic modal models were created, one for the cavity of the cylinder and the other for the interior volume of the VAD. Since the VAD structure was already present in the FEM, it was decided to calculate one complete FE model of the structure, rather than using a separate model for the cylinder, the mass/spring of the TMD and another of the diaphragm of the VAD. This also lead to a reduction in the solution times. This approach will not be suitable for Stage 2 since the positions of the VAD's will need to be continually moved and would require recalculation of the modal response each time a VAD is moved. The other advantage of coupling the VAD to the panel and solving for the whole structure was that local effects around the spring connection points could be easily studied. It was found that this was very important (see Section 4.3).

Therefore for stage 2 of the project, smaller VAD's will be used. This will allow a single acoustic model to be used. The modal coupling theory will be used to then connect the structural and acoustic modal models of the VAD to the modal models of the cavity and structure.

3.6 Comet and the External Pressure Field

The objective of this task was to develop methods to predict the external pressures on the surface of the launch vehicle, or appropriate model test rigs. COMET version 4.0 Boundary Element Analysis (BEA) software has been used. The code has been validated against analytical solutions, and the range of accuracy and size of problem that can be solved given current resources has been established.

3.6.1 Comet BEM Software

The COMET version 4.0 Boundary Element Analysis (BEA) software[15] has been used to predict the external pressures on the surface of the cylinder. COMET is a commercial BEA program that utilises a preprocessor such as ANSYS to generate the boundary element mesh. Appendix B (and Morgans[16]) describes the technique more fully and validates it by comparing it to the analytical solution for scattering from a sphere.

The conclusions from this work are that for a scattering type problem, the following BEA analysis procedure should be followed:

- use a direct method of BEA analysis,

- use an element / wavelength density of 12 for the most accurate results, although reasonable, but less accurate, results can be obtained by using element / wavelength spacings down to 6.

- use standard quadrature,
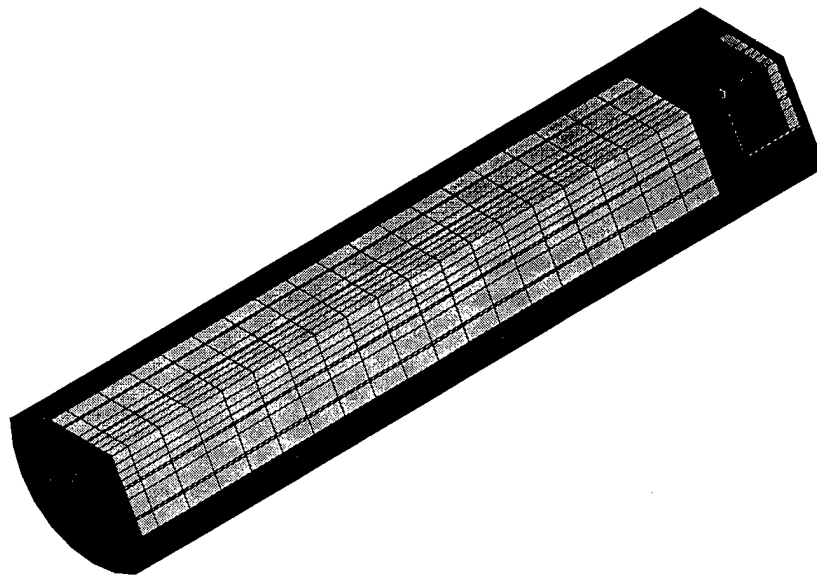
(a) Full FEM
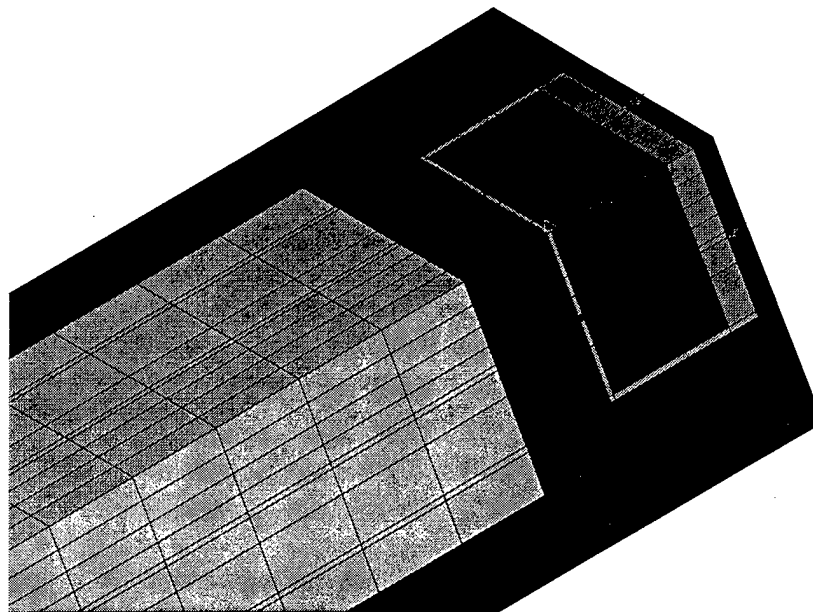
(b) Zoom around the VAD

Figure 12: Finite element model of the cylindrical structure with the internal cavity and VAD. The cylindrical shell elements are not displayed here. The colours of the elements represent the element type; Cyan are the acoustic elements without structural DOF's, Purple are the acoustic elements with structural DOF's, Red are the diaphragm elements, Green are the elements forming the VAD walls. The diaphragm and VAD springs (shown as coils) are Magenta and Light Blue respectively. The diaphragm and VAD masses (shown as small squares) are Light Green and Purple respectively.

- use CHIEF over-determination at frequencies corresponding to the internal natural modes.

3.6.2 Problem Specification

The first experimental test rig uses a loudspeaker as a sound source, situated 1 m away from the aluminium plate, on the axis of the cylinder.

This is modeled as a monopole source. The problem could be considered to be "end-on scattering from a finite cylinder". The dimensions of this cylinder are approximately 0.5 m diameter x 2 m long.

The dimensions of the second Boeing test ring are approximately 3 m diameter x 4 m long, while the dimensions of the Minotaur launch vehicle appear to be in the order of 1.5 m diameter x 5.3 m long. The frequency range of interest is 0 - 400 Hz.

3.6.3 Resource usage

Resource usage and scaling of solution times is critical in this application, as typically one would have to solve the harmonic problem at each frequency of interest. The plot in Figure 13(a) shows the logarithm of the problem size (or number of elements) verses the logarithm of the solution time for a single frequency. The points on the graph represent typical problem sizes, starting with the small cylinder with low accuracy, small cylinder with high accuracy, launch vehicle with low accuracy, and Boeing test with low accuracy. It can be seen that the time required increases rapidly with the number of elements (to the power of ~3).

For the calculations with the CHIEF method, the largest run was out of memory by 0.3 of a mega-word. This implies that problems in the order of 131M words are the limit for the currently compiled version of COMET, and that by reducing the problem size slightly (maybe 4 CHIEF points instead of 6, or a slightly less dense mesh) this problem could be solved. The extrapolated time would be in the order or 7700 CPU seconds (2.1 CPU hours).

A similar trend is seen with memory usage in Figure 13(b).

The time taken for the largest problem is in the order of 2.1 CPU hours per frequency. This means that with this technique it is possible to produce results, but it will take considerable time. However the calculations will only have to be performed once per geometry.

At the time of these calculations, the limit for an NT based COMET executable for an in core solution was 32 M words (~128 M bytes). If an executable could be made at least double this then full use could be made of available RAM and solutions times should decrease (to maybe a power of 2 function).

3.6.4 Alternative techniques

Alternative techniques for calculating the external pressure were considered in light of the time taken to calculate the solution for large models. Due to the acquisition of a larger machine and a larger (128 M word) COMET executable, these alternatives were deemed not necessary.

3.6.4.1 Axi-symmetric BEA   The geometries considered are generally axi-symmetric. If the loading could be considered to be entirely axi-symmetric, then an axi-symmetric BEA approximation could be made. COMET does not support 2D calculations at this stage. It does however support planes of symmetry, and it may be possible to reduce processing time at the cost of complexity of implementation.
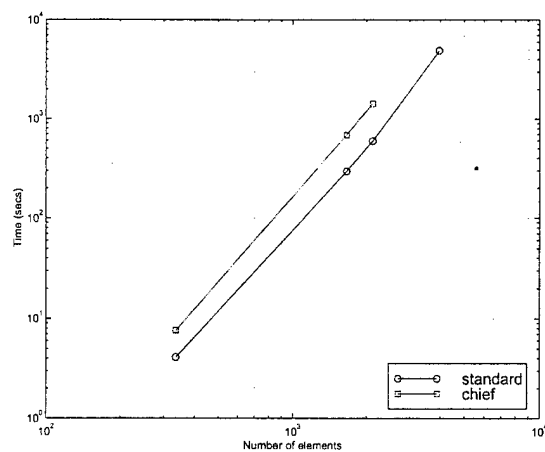
(a) Runtime of BE model vs problem size
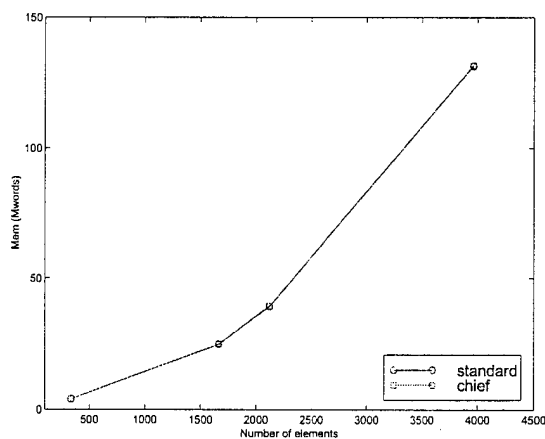
(b) Full incore momory usage for BE method vs problem size

Figure 13: Time taken and memory used for typical COMET simulations used in this study.

3.6.4.2 FEA Again if the geometry and loading could be considered to be entirely axi-symmetric, it may be more economical to calculate the element surface pressures by a 2D axi-symmetric FEA calculation. This would involve meshing the exterior of the domain and using far field elements to make sure no waves were reflected from the truncated "infinite" boundary.

3.6.4.3 Analytical Although analytical solutions do exist for simple sources scattering off simple regular geometries, these techniques are not suitable for more complex shaped bodies. Consequently, analytical solutions were not investigated.

3.6.5 Calculation of the External Pressure Field

ANSYS macros have been written that generate COMET input files for the geometry and, if required the COMET data recovery mesh (a mesh of nodes or "virtual microphones" required for post-processing external field data).

COMET results are calculated for 40 frequencies in the range of interest, using the recommended BEA analysis techniques (Appendix B). The element results files are then filtered through a custom filter written in PYTHON, spatially and frequency interpolated in MATLAB and post-processed in ANSYS to produce an equivalent nodal force for input as a boundary condition for the next stage of the modeling.

3.6.5.1 Spatial Interpolation of the External Pressure Field Given the resource requirements for future stages of the project, it was decided to implement a spatial interpolation routine. This alleviates the need for a coincident COMET surface pressure mesh and ANSYS surface structural mesh, which must be fine enough to capture the structural modes accurately.

3.6.5.2 Frequency Interpolation of the External Pressure Field Calculating the external pressure field over the surface of the cylinder for each frequency between 0Hz and 400 Hz was infeasible due to the long solutions times. Therefore, a (frequency domain) interpolation procedure was used to interpolate between solutions with a coarse frequency spacing. In order to achieve an accurate solution when interpolating between frequencies, it is necessary to ensure that the maximum change in the phase between adjacent frequencies (solutions) for any particular node on the surface of the structure should not be more 60 degrees[17].

The biggest phase shifts are at the structural nodes furthest from the source. Assuming that the length from the source to the furthest node is x, then the phase angle at these nodes is $\arg(e^{i2\pi\frac{fx}{c_0}})$. The difference in phase between adjacent solutions must be less than $60°$, ie
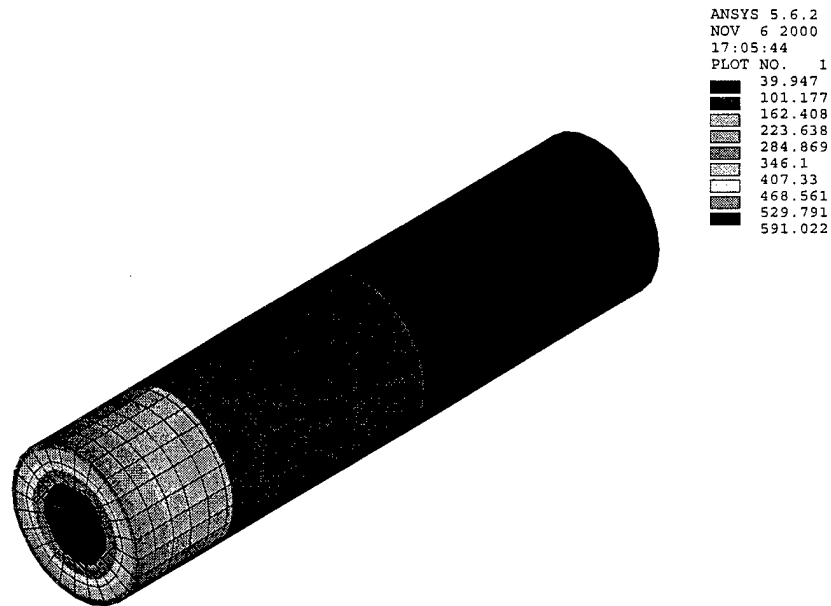
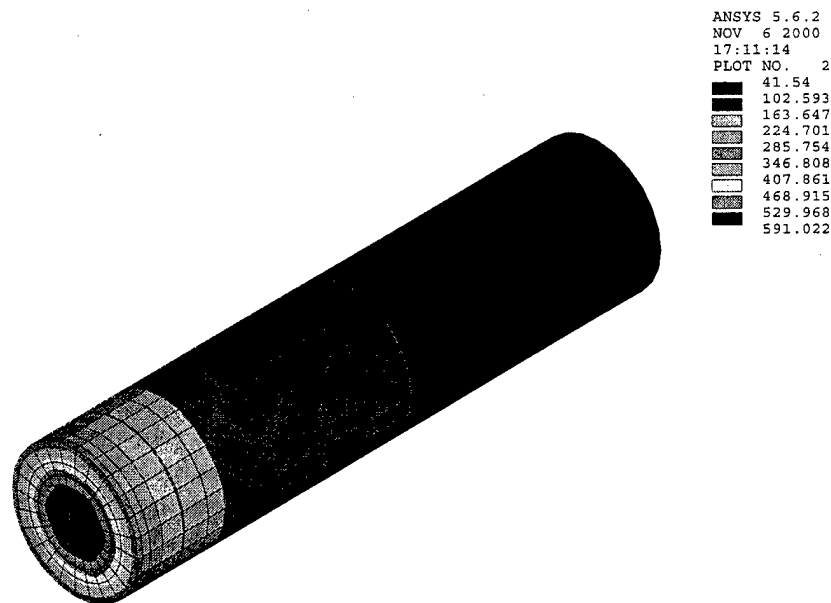$$\frac{2\pi x}{c_0}(f_{n+1} - f_n) < \frac{\pi}{3} \tag{47}$$

and therefore,

$$\Delta f = f_{n+1} - f_n = \frac{c}{6x} \tag{48}$$

The number of frequency points for the interval from 0 Hz to f_{max} is given by

$$n = \frac{f_{max}}{\Delta f} \tag{49}$$

(a) Comet BE model and surface pressures

(b) Ansys FE model and surface pressures

Figure 14: Illustration of spatial interpolation. Comparison of different meshes and calculated pressures for the COMET model and final ANSYS model at the worst case frequency of 400Hz.

For example, a maximum frequency of 400 Hz and 4m acoustic path (cylinder length of 2.14m, source to front end cap is 1m), the minimum number of required points is approximately 28.

The nodal forces were calculated using COMET at 41 frequencies from 0 Hz (0.5Hz) to 400 Hz in 10 Hz steps. The frequency domain interpolation of the structural forces was done in MATLAB (**interp2**). Using a *bicubic* interpolation routine the forces were then interpolated for each frequency from 1 Hz to 400 Hz. The results of the interpolation are shown graphically in Figure 15. Results were accurate to at least 4 significant figures.
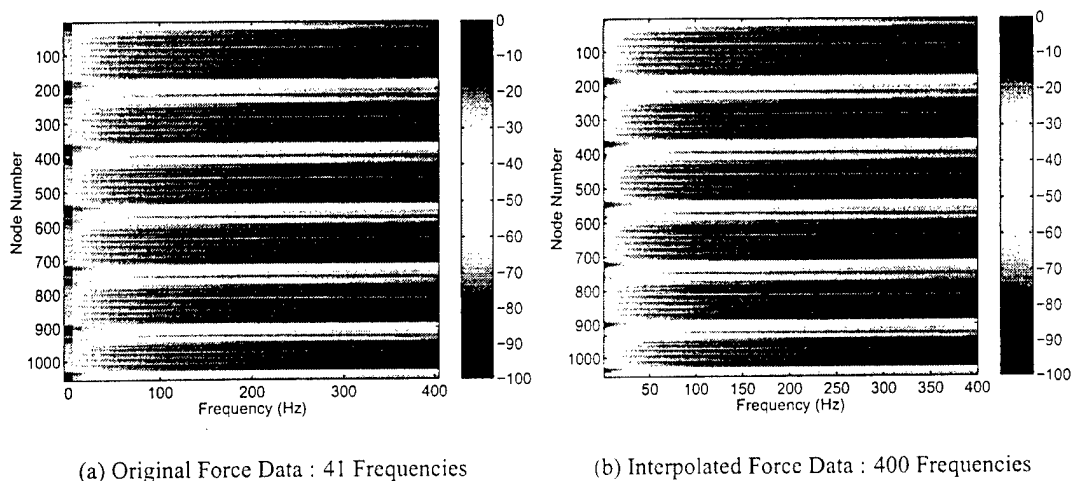

(a) Original Force Data : 41 Frequencies   (b) Interpolated Force Data : 400 Frequencies

Figure 15: Illustration of the frequency domain interpolation routine.

4   VAD Performance

With the model and modelling technique validated, various VAD configurations were investigated in an attempt to find an optimal design to reduce the overall space averaged sound pressure level transmitted into the cavity from an external acoustic source.

4.1   The external acoustic source

The external pressure field was generated by a monopole acoustic source located on axis 1m from the flexible panel. The results were generated in COMET at 41 frequencies and then imported into MATLAB to provide an equivalent force to all the external structural nodes. The sound field was then interpolated at all 400 frequencies, that is from 1 Hz to 400 Hz in steps of 1 Hz).

4.2   Optimisation of the VAD

Three basic VAD configurations were investigated, the first two were shown in Section 3.5.1, the only difference being that one had a flexible diaphragm and the other had a stiff diaphragm (essentially a tuned mass device). The third model had the VAD rotated 180 degrees as shown in Figure 16.
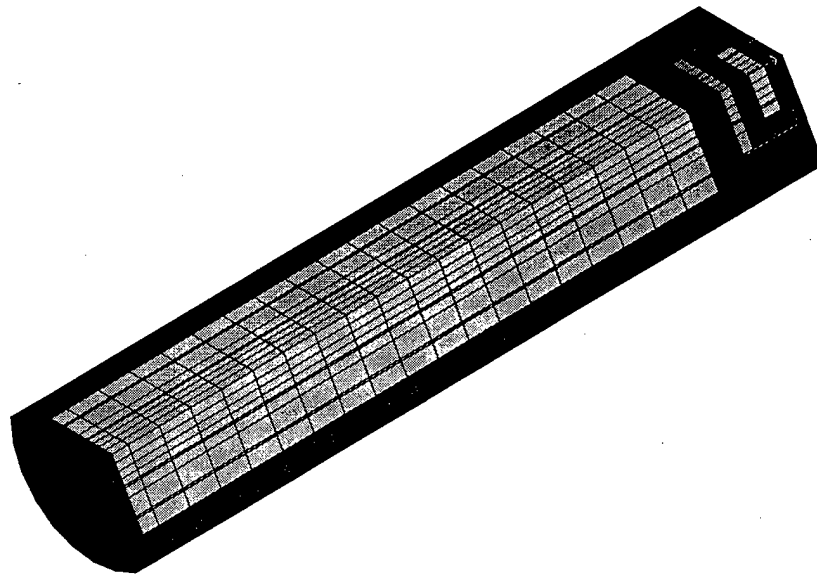
(a) Full FEM
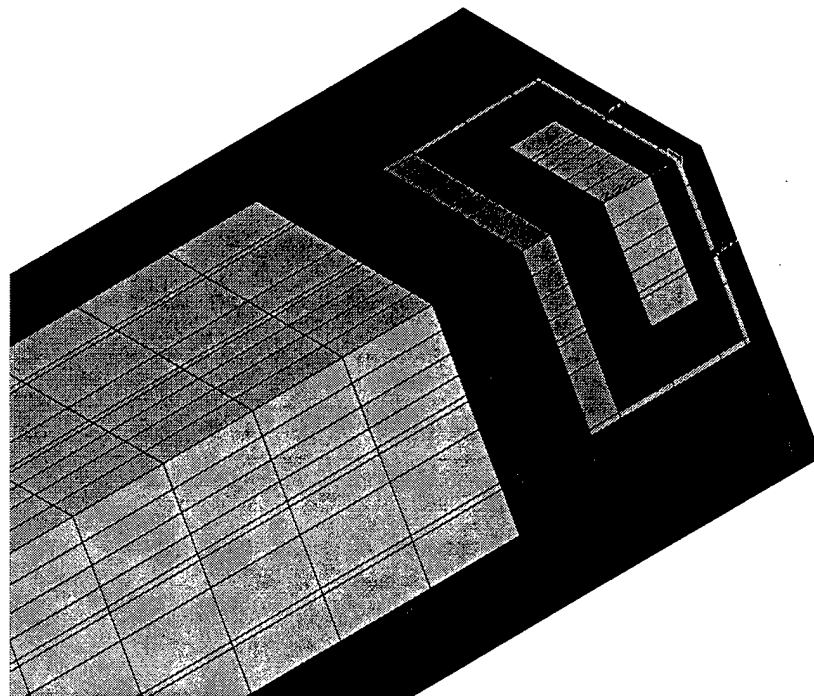
(b) Zoom around the VAD

Figure 16: Finite element model of the cylindrical structure with the internal cavity and the rotated VAD. The cylindrical shell elements are not displayed here. The colours of the elements represent the element type; Cyan are the acoustic elements without structural DOF's, Purple are the acoustic elements with structural DOF's, Red are the diaphragm elements, Green are the elements forming the VAD walls. The diaphragm and VAD springs (shown as coils) are Magenta and Light Blue respectively. The diaphragm and VAD masses (shown as small squares) are Light Green and Purple respectively.

Many configurations of VAD parameters were investigated and the effect they had on the overall acoustic potential energy was calculated. The detailed results of these studies can be found in Appendix C. The results presented below form a summary of the key findings and an optimal design approach.

4.2.1 Empty Cylinder

The performance of the following empty cavity configurations were investigated:

- Baseline empty cavity,

- Double the damping (both cavity and structural)

- Added mass (2 kg) smeared across the flexible panel and at the same time keeping the resonance frequency constant,

- Added mass (2 kg) smeared across the flexible panel, but leaving the stiffness the same.

The results are shown in Table 7. The equivalent data is shown graphically in Figure 17. The damping was achieved by increasing the modal loss factors of the cavity and the structure to 7% and 4% respectively. The third case was simulated by increasing the modal mass of the panel modes by 0.5kg (one quarter of 2kg). The final case had the modal mass increased by 0.5 kg and the resonance frequencies were decreased accordingly. It can be seen that conventional sound control measures such as adding mass and damping are somewhat effective. The additional mass only is the most effective control measure since it brings down the natural frequency of the fundamental panel mode. In doing so, the mode is less efficient at transmitting energy to the higher order acoustic modes.

Case	Acoustic Potential Energy (dB)
Empty Cavity Baseline	**47.6 | 49.6**
Double Damping	44.5 | 46.8
Increased Mass (constant res. freq.)	40.3 | 41.8
Increased Mass	35.9 | 36.6

Table 7: Sound transmission for the various empty cavity configurations. Tabulated values are the acoustic potential energy band averaged for 50 to 200 Hz and 50 to 400 Hz. The baseline configuration is shown in bold type face.

4.2.2 Cylinder with VAD

For lightly damped resonators, that is mostly reactive, it was found that the optimal reduction in acoustic energy within the cavity for the entire frequency band may achieved by pushing the resonance frequencies of the system outside the band of interest. To achieve this, the fundamental panel mode needed to be below 50 Hz and the coupled asymmetric panel/TMD mode needed to be above 400Hz. In fact, ideally the anti-resonance associated with these two modes should lie somewhere in the middle of the band. The best results appear to come from a mis-tuned
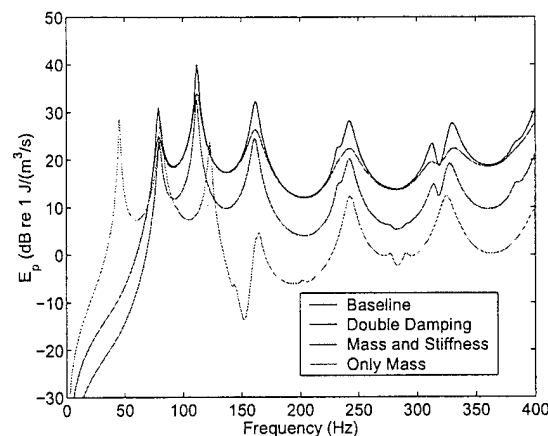
Figure 17: Sound transmission for the various empty cavity configurations.

device, with the uncoupled TMD mode at about 600Hz. It should be noted that this was only effective because the energy flux from the exterior of the cavity to the interior was dominated by the fundamental panel mode. In the cases where additional efficiently radiating structural modes exist, additional reactive structural devices may be required.

Heavily damped resonators that are essentially absorptive devices are very effective at coupling into specific modes, be they acoustic or structural, and reducing the modal participation factors of these modes at resonance. This type of approach could be very effective at increasing the damping of the acoustic modes at low frequencies, something very difficult to achieve in practice with thin absorptive materials.

The performance of the baseline TMD and VAD configuration, as well as more optimal configurations is shown in Table 8. The equivalent data is shown graphically in Figures 18(a)-(c). It can be seen that the largest reductions occur when the in-phase and out-of-phase plate/TMD modes are shifted beyond the frequency band of interest. The diaphragm is effective at reducing the amplitude of the fundamental cavity mode, although in this particular case, this mode does not contribute strongly to the overall band averaged levels. Possibly in a different system the effect would be more pronounced.

4.3 Alternative Designs

The simulations in the previous section showed that it was possible to achieved significant gains in performance by increasing the VAD spring stiffness; however, when the modal models of the structure were re-calculated in ANSYS with the modified spring stiffness, and then reanalysed in MATLAB, the performance gains were not realised. It was found that the panel suffered from localised bending and subsequently was unable to provide sufficient stiffness to move the out-of-phase mode beyond the frequency band of interest (see Figure 19a).

Therefore in light of these findings, several modified FE models were considered with alternative spring arrangements so as to reduce the local flexure around the springs. Two successful designs used seven springs (with a spring stiffness of 3/7 to keep the overall spring stiffness constant) rather than the three used for the earlier FE models. Figures 19(b) and 19(c) shows the FE models and the out-of-phase mode shapes of the two alternative designs. The difference between the FE models in Figures 19(b) and 19(c), is that the former model had 6 springs attached at a radius of 80 mm with an additional spring in the centre, whereas the latter model

Case	Acoustic Potential Energy (dB)
Empty Cylinder	**47.6 | 49.6**
TMD Baseline	**28.8 | 51.3**
VAD Baseline	**30.1 | 51.4**
Reversed VAD Baseline	29.3 | 50.7
TMD: $f_{TMD} = 600\text{Hz}$, $\eta_{TMD} = 0.06$	19.7 | 35.6
TMD: $f_{TMD} = 111\text{Hz}$, $\eta_{TMD} = 0.20$	28.5 | 48.1
VAD: $f_{TMD} = 600\text{Hz}$, $\eta_{TMD} = 0.06$, $f_d = 80$ Hz, $\eta_d = 0.2$	22.9 | 35.6
VAD: $f_{TMD} = 111\text{Hz}$, $\eta_{TMD} = 0.2$, $f_d = 80$ Hz, $\eta_d = 0.2$	29.9 | 48.2
Reversed VAD: $f_{TMD} = 600\text{Hz}$, $\eta_{TMD} = 0.06$, $f_d = 80$ Hz, $\eta_d = 0.2$	19.6 | 34.2
Reversed VAD: $f_{TMD} = 111\text{Hz}$, $\eta_{TMD} = 0.2$, $f_d = 80$ Hz, $\eta_d = 0.2$	26.2 | 47.4
Seven Springs VAD*: $f_{TMD} = 600\text{Hz}$, $\eta_{TMD} = 0.20$, $f_d = 80$ Hz, $\eta_d = 0.2$	28.2 | 43.6
Seven Springs VAD Alternative*: $f_{TMD} = 600\text{Hz}$, $\eta_{TMD} = 0.20$, $f_d = 80$ Hz, $\eta_d = 0.2$	36.7 | 37.6

Table 8: Sound transmission with the variations of the VAD attached to the cylinder. Tabulated values are the acoustic potential energy band averaged for 50 to 200 Hz and 50 to 400 Hz. The baseline configurations are shown in bold type face. f and η are the natural frequency and the modal loss factor of the uncoupled modes, the subscript TMD and d refer to the tuned mass device and diaphragm respectively. * See Section 4.3.

(a) Tuned Mass Device

(b) Vibro Acoustic Device

(c) Reversed Vibro Acoustic Device
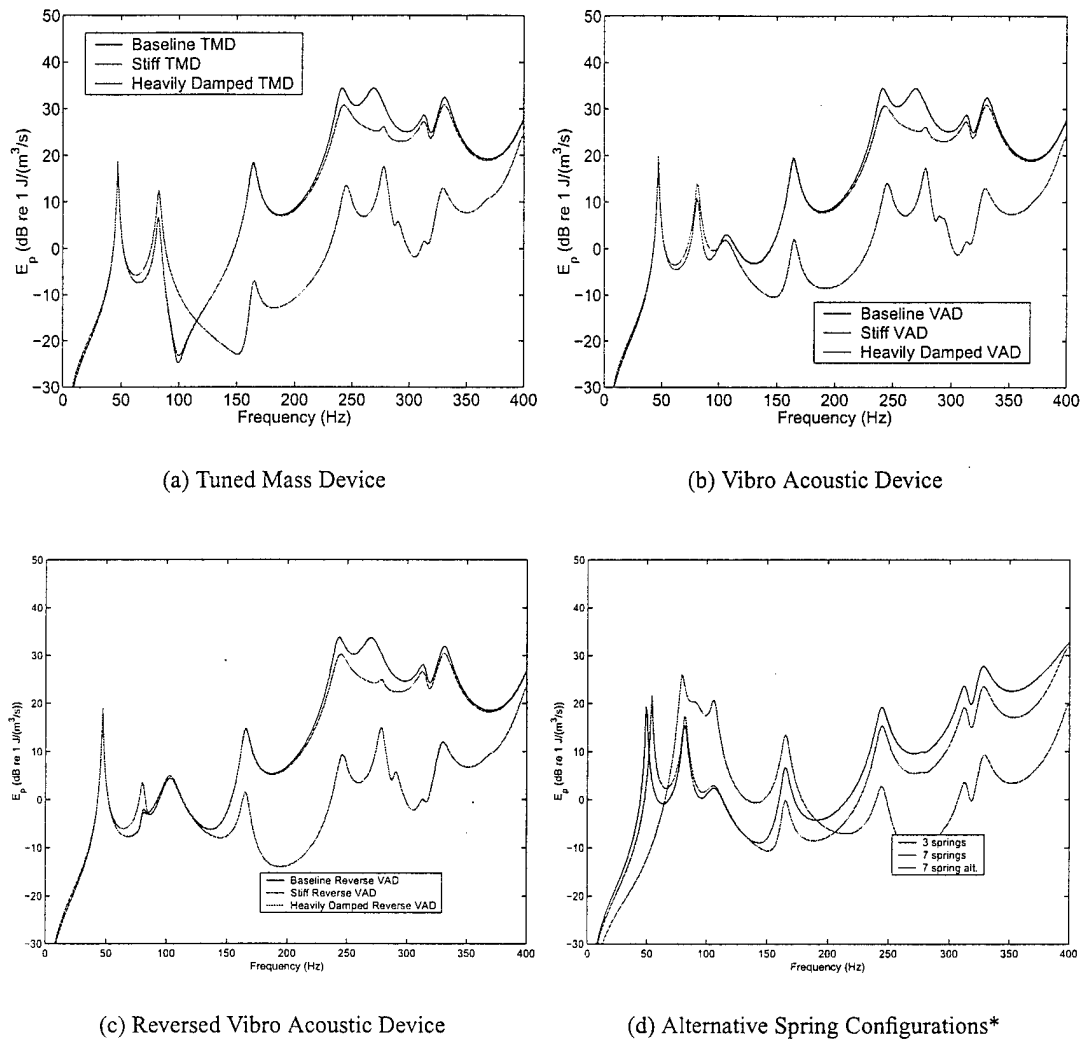
(d) Alternative Spring Configurations*

Figure 18: Sound transmission with the variations of the VAD attached to the cylinder. *See Section 4.3.

had the 6 springs attached at a radius of 147 mm making it slightly stiffer. The figure also lists the coupled out-of-phase natural frequencies of the three models. It can be seen that the seven spring arrangements have successfully moved the natural frequency of the out-of-phase mode outside the frequency band of interest.

The sound transmission into the cavity with the three different spring arrangements can be seen in Figure 18(d). The alternative spring arrangement has greatly reduced the high frequency noise levels but at the expense of the low frequencies. The single band averaged levels for this arrangement are somewhat poor since the fundamental panel mode resonance frequency is no longer below the 50 Hz threshold. The addition of a small amount of mass would overcome this.

Therefore, when designing such devices it it necessary to keep in mind the local stiffness of the attachment points. In practice it might be best to place the VAD's on the ribs of the structure where the local stiffness is high.

(a) 3 Spring : 386 Hz

(b) 7 Spring : 427 Hz

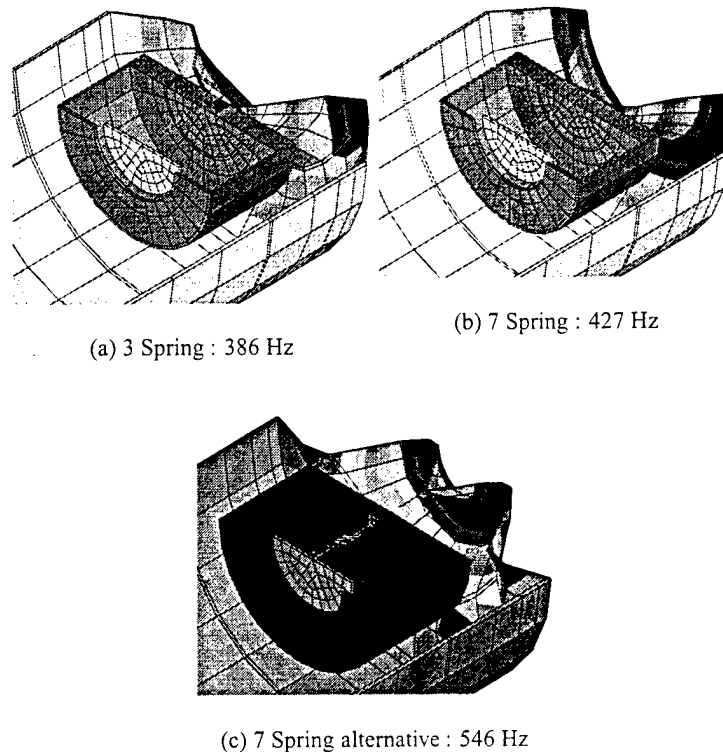(c) 7 Spring alternative : 546 Hz

Figure 19: Finite element model showing the mode shapes of the out-of-phase mode for the 3 different spring configurations. The coupled resonance frequencies are shown and are for an uncoupled VAD resonance frequency of 600Hz.

4.4 Summary

It appears from the simulations that for the particular system under investigation, the optimal design for the VAD is to use the TMD component in a mostly reactive mode. The coupled TMD / panel then has, an in-phase mode where mass loading reduces the coupled resonance

frequency below the lower frequency bound (50 Hz), and an out-of-phase mode where stiffness loading increases the coupled resonance frequency above the upper frequency bound (400 Hz).

The diaphragm mode of the VAD can be used to selectively "kill" a single acoustic mode. This may be an efficient way of introducing acoustic damping at low frequencies where conventional absorptive materials are limited.

5   Conclusions

The objectives of the study have been achieved. A numerical framework for the study of the response of an irregularly shaped vibro-acoustic system excited by an external pressure field has been developed. The method used the modal coupling technique which coupled the *in-vacuo* modal model of the structure to the rigid-walled modal model of the cavity. The solution times of the (modal coupling) method were found to be extremely fast, solving two to three orders of magnitude faster than a fully coupled FEA. The modal coupling technique was validated against a fully coupled FEA. The FE model of the structure was adjusted so as to accurately emulate the physical structure. The effect of the VAD was analysed and optimised for two bandwidths, namely 50-200Hz and 50-400Hz. It was found that the optimal VAD design used the TMD as a highly reactive device to reduce the structural modal density within the frequency band of interest and the optimal diaphragm configuration was highly lossy to reduce the modal amplitude of a single acoustic mode. Local flexure of the panel reduced the effectiveness of the VAD's and alternative attachment techniques were investigated to reduce such flexure. The broadband noise reductions in the space averaged sound levels with the optimised VAD was 12dB.

References

[1] C.H. Hansen, A.C. Zander, and C.Q. Howard. Investigation of passive control devices for potential application to a launch vehicle structure to reduce the interior noise levels during launch. Progress report, The University of Adelaide, 2000.

[2] R.H. Lyon and G. Maidanik. Power flow between linearly coupled oscillators. *Journal of the Acoustical Society of America*, 34:623, 1962.

[3] F.J. Fahy. Vibration of containing structures by sound in the contained fluid. *Journal of Sound and Vibration*, 10(3):490–512, 1969.

[4] L.D. Pope. On the transmission of sound through finite closed shells: Statistical energy analysis, modal coupling, and non-resonant transmission. *Journal of the Acoustical Society of America*, 50(3):1004–1018, 1971.

[5] E.H. Dowell, G.F. Gorman III, and D.A. Smith. Acoustoelasticity : General theory, acoustic natural modes and forced response to sinusoidal excitation, including comparisons with experiment. *Journal of Sound and Vibration*, 52(4):519–542, 1977.

[6] F. Fahy. *Sound and Structural Vibration: Radiation, Transmission, and Response*. Academic Press, London, 1985.

[7] M. Humi and W.B. Miller. *Boundary Value Problems and Partial Differential Equations*. PWS-Kent, Boston, 1992.

[8] S.D. Snyder and C.H. Hansen. The design of systems to actively control periodic sound transmission into enclosed spaces, Part 1: Analytical models. *Journal of Sound and Vibration*, 170(4):433–449, 1994.

[9] Matlab 5.4. *Matlab User Guide*. Mathworks, 5.4 edition, 1998.

[10] J. Pan. The forced response of an acoustic-structural coupled system. *Journal of the Acoustical Society of America*, 91(2):949–956, 1992.

[11] L.P. Fanzoni and E.H. Dowell. On the accuracy of modal analysis in reverberant acoustic systems with damping. *Journal of the Acoustical Society of America*, 97(1):687–690, 1995.

[12] L.P. Fanzoni and D.B. Bliss. A discussion of modal uncoupling and an approximate closed-form solution for weakly coupled systems with application to acoustics. *Journal of the Acoustical Society of America*, 103(4):1923–1932, 1998.

[13] V. Jayachandran, S.M. Hirsch, and J.Q. Sun. On the numerical modelling of interior sound fields by the modal expansion approach. *Journal of Sound and Vibration*, 210(2):243–254, 1998.

[14] A.W. Leissa. *Vibration of Plates*. ASA, 1973.

[15] Automated Analysis Corporation. Comet Users Guide.

[16] R. Morgans. External Acoustic Analysis Using COMET. Internal report, The Department of Mechancial Engineering, Adelaide University, July 2000.

[17] F. Fahy. *Sound Intensity*. E&FN Spon, London. 2nd edition, 1995.

[18] P.M. Morse and K.U. Ingard. *Theoretical Acoustics*. Book. McGraw-Hill Book Company, New York, 1968.

A   Verification of Modal Coupling

In order to have any confidence in the numerical simulations it was necessary to validate the modal coupling (derived in Section 2) software written in MATLAB. The contiguous cylinder/cavity system shown in Figure 20 was used as the model for the verification.
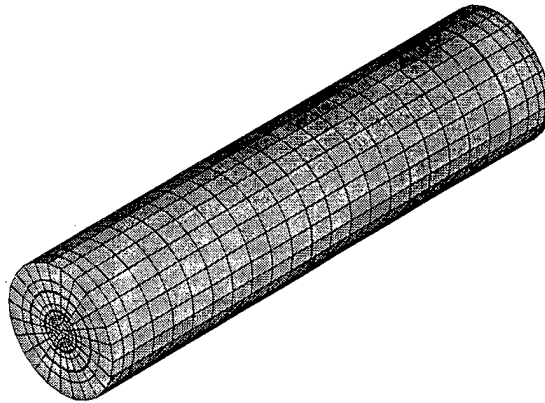

Figure 20: Finite element model of the coupled curved panel/cavity system used to validate the modal coupling code in MATLAB.

The displacement dofs not associated with the nodes of the structure were set to 0 to reduce the bandwidth of the frontal solver (solution effort). By default, boundary conditions for the external nodes of the fluid elements have zero pressure gradient normal to the surface, ie $\partial p / \partial \hat{n} = 0$.

The MATLAB code was verified in two stages

- Uncoupled - Structure only and Cavity only

- Fully Coupled vibro-acoustic system using modal coupling theory.

The panel and the cavity were modelled individually using the FEA package ANSYS. A modal analysis was performed on both of the models and the modal data were then exported in a form that could be read into MATLAB. It has been assumed that the modal analysis results from ANSYS were valid (the objective here was to test the modal coupling not the accuracy of the modal solver).

A forced response simulation was performed using a modal superposition technique on the uncoupled modal models using both ANSYS and MATLAB and the results were compared.

Once the uncoupled models were validated including the *ad hoc* damping terms, a fully coupled forced response analysis was performed using ANSYS. This was then compared against the coupled acoustic and structural models via modal coupling theory[8] within MATLAB.

There was no attempt to verify that the results from either ANSYS or MATLAB reflected the physical system upon which the models were based. The sole purpose was to verify that the assumptions to the system of equations and the software code were accurate.

A.1   Uncoupled Response Analysis

The structure and the cavity models were analysed separately. A finite number of modes were extracted in ANSYS and these were used as the basis for a modal superposition analysis within both ANSYS and MATLAB.

A.1.1 Forced Response of Structure Only

The first 54 structural modes below 800 Hz were extracted from the FE model, of which, the first 20 natural frequencies (below 400Hz) are shown in Table 9. The forced response simulation of the panel used a unit force applied to the centre of the panel at node 1 ([0,0,0]) as shown in Figure 20. This symmetric location was chosen to ensure that only the odd order structural modes were driven. Should any of the even modes be driven then this would indicate that either the model or the modelling procedure was at fault. It also clearly shows the effect that modal coupling has on the excitation of additional modes (see Section A.2).

Mode	Natural Frequency
1	55.7
2	111.5
3	124.7
4	140.6
5	195.7
6	206.1
7	232.7
8	232.8
9	246.2
10	274.0
11	280.8
12	286.4
13	318.9
14	353.9
15	366.5
16	366.7
17	383.5
18	383.5
19	396.7
20	407.0

Table 9: Natural frequencies of the first 20 structural modes.

Figure 21 shows the structural impedance of the panel when driven normal to the surface at the geometric centre (node 1) as shown in Figure 20. The response point was also located at node 1. The system was undamped.

As can be seen the forced response results from ANSYS and MATLAB are identical. Figure 22 shows the results of the forced response simulations using the same system and conditions as before with the exception that structural damping with a modal loss factor, η, of 2%, has been
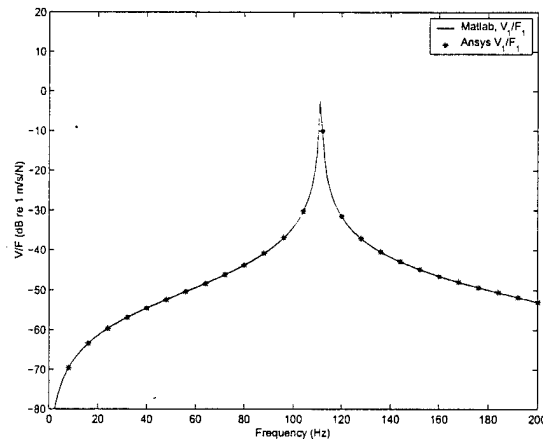
Figure 21: Structural impedance of the panel when driven in the centre, $\eta = 0$

applied. Again, both the ANSYS and MATLAB results are identical. Thus it can be concluded that the modal response for the structure is calculated correctly within MATLAB.
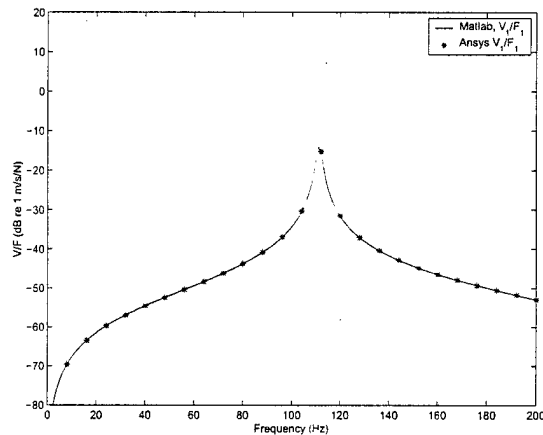

Figure 22: Structural impedance of the panel when driven in the centre, $\eta = 2\%$

### A.1.2 Forced Response of Cavity Only

The first 40 acoustic modes were extracted from the FE model, of which, the first 10 are shown in Table 10. The forced response simulation of the cavity used a unit volume velocity applied at the surface of the centre of the flexible panel (cavity node 1). Two response points were used; one at the excitation point and another at the opposite end of the cavity (node 175) as shown in Figure 20.

Figure 23 shows the acoustic impedance of the cavity when driven as shown in Figure 20. As can be seen the cavity forced response results from ANSYS and MATLAB are identical.

Figure 24 shows the results of the forced response simulations using the same system and conditions as before with the exception that viscous damping has been applied, with a modal loss factor, η, of 2%. Again, both the ANSYS and MATLAB results are identical. Thus it can be concluded that the modal response for the cavity alone is calculated correctly within MATLAB.

Mode	Natural Frequency
0	1E-04
1	80.3
2	161.0
3	242.4
4	324.9
5	398.5
6	398.5
7	406.5
8	406.5
9	408.8

Table 10: Natural frequencies of the first 10 cavity modes.
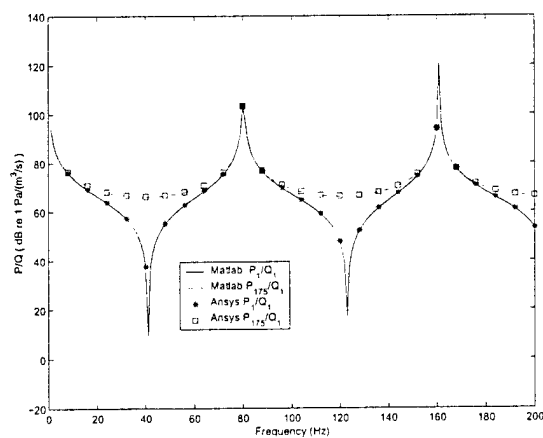
Figure 23: Acoustic impedance of the cavity when driven at the surface of the flexible panel centre with an acoustic source, $\eta = 0$
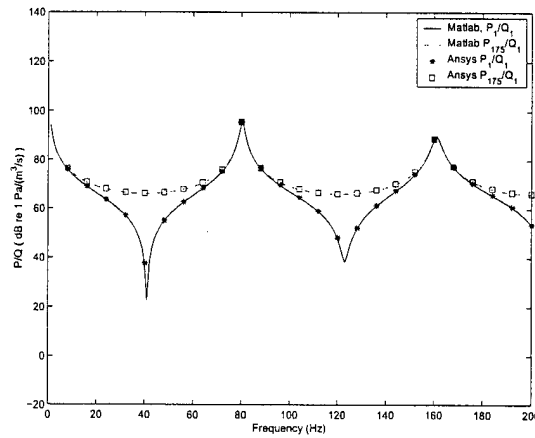
Figure 24: Acoustic impedance of the cavity when driven at the surface of the flexible panel centre with an acoustic source, $\eta = 2\%$

A.2   Coupled Response Analysis

The FE models of the cavity and structure were coupled within ANSYS, resulting in the following homogeneous equation

$$\left[\begin{bmatrix} \mathbf{K}_s & \mathbf{K}_{fs} \\ 0 & \mathbf{K}_p \end{bmatrix} - \omega^2 \begin{bmatrix} \mathbf{M}_s & 0 \\ \mathbf{M}_{fs} & \mathbf{M}_p \end{bmatrix} + j\omega \begin{bmatrix} \mathbf{C}_s & 0 \\ 0 & \mathbf{C}_p \end{bmatrix} \right] \begin{bmatrix} \mathbf{u} \\ \mathbf{p} \end{bmatrix} = [0] \tag{50}$$

where the subscripts s and p refer to the structure and cavity respectively, $\mathbf{K}$, $\mathbf{M}$ and $\mathbf{C}$ are the stiffness, mass and damping matrices respectively, $\mathbf{u}$ is the nodal displacement vector and $\mathbf{p}$ is the nodal pressure vector. The unsymmetric sub matrices $\mathbf{K}_{fs}$ and $\mathbf{M}_{fs}$ are the coupling stiffness and mass matrices respectively. The solution of the unsymmetric system of equations leads to much larger solution time than for similar sized models which have a symmetric formulation (such as the uncoupled models).

The current release of ANSYS (version 5.6) used for the verification process did not have the facility to evaluate the forced response of a coupled system using a the modal superposition technique outlined in Section 2. Rather the harmonic response solver directly solves the following system of equations

$$\left[\begin{bmatrix} \mathbf{K}_s & \mathbf{K}_{fs} \\ 0 & \mathbf{K}_p \end{bmatrix} - \omega^2 \begin{bmatrix} \mathbf{M}_s & 0 \\ \mathbf{M}_{fs} & \mathbf{M}_p \end{bmatrix} + j\omega \begin{bmatrix} \mathbf{C}_s & 0 \\ 0 & \mathbf{C}_p \end{bmatrix} \right] \begin{bmatrix} \mathbf{u} \\ \mathbf{p} \end{bmatrix} = \begin{bmatrix} \mathbf{F}_s \\ \mathbf{F}_p \end{bmatrix} \tag{51}$$

This unsymmetric formulation requires the use of an unsymmetric solver which greatly increases the solution times and makes the use of a fully coupled analysis extremely unattractive. When drawing comparisons between the modal superposition and fully coupled solutions it must be remembered that the modal superposition technique is evaluated for a limited set of modes, whereas the fully coupled technique is effectively evaluated over an "infinite" set of modes. Therefore, at resonance when only a single mode dominates the response the solutions should be equal. However, off resonance the solutions may differ, particularly at the anti-resonances where the residues of the higher order modes may contribute to the stiffness of the fully coupled system. As the stiffness residue term is increased (by accounting for more modes) the frequencies at which the anti-resonances occur is reduced.

A.2.1   Forced Response of the Structure with Coupled Cavity

As with the uncoupled case, the curved panel was driven with a unit force in the centre of the panel (node 1). The drive point structural impedance was calculated within ANSYS by solving the fully coupled expression given by Equation (51) and also by using the modal coupling technique in MATLAB. The results from the two techniques are shown as a drive point structural impedance and force to pressure transfer function in Figures 25 and 26 respectively.
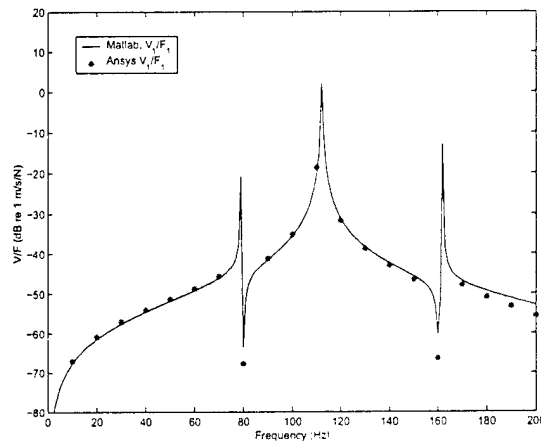
Figure 25: Drive point structural impedance of the coupled system

Looking at Figure 25 it is clear that the modal coupling theory is accurately predicting the behaviour of the coupled system. The resonances from the two simulations are well aligned. The slight discrepancies seen at the anti-resonances are to be expected, particularly at the high frequency end, and they are due to an inadequate number of structural and/or acoustic modes used for the simulation within MATLAB. It should also be noted that due to the long time taken for the simulations within ANSYS, the frequency spacing is coarse (10 Hz) and subsequently the magnitudes near the resonances are not necessarily accurate.
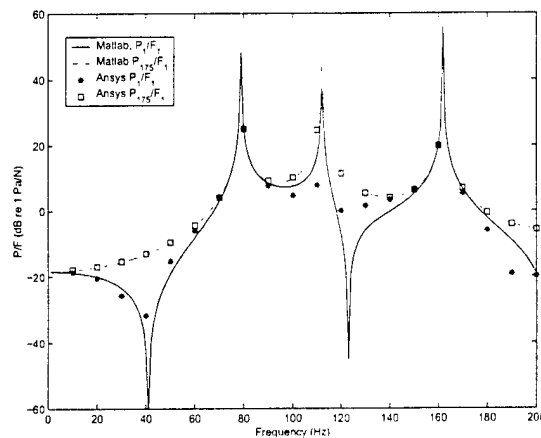
Figure 26: Pressure / Force transfer function of the coupled system

Figure 26 also shows that the MATLAB simulation did not have sufficient modes to model the residues from the higher order modes. This is not such an issue for noise control simulations

as the regions around the anti-resonances contribute very little to the overall energy transmission from one subsystem to another.

A.2.2   Forced Response of the Cavity with Coupled Structure

As with the uncoupled case, the cavity was driven at the centre of the panel surface (at node 1) with a unit volume velocity. The system response was calculated within ANSYS by solving the fully coupled expression given by Equation 51 and also by using the modal coupling technique in MATLAB. The results from the two techniques are shown as acoustic impedances between nodes 1 and 175 to node 1 in Figure 27. The volume velocity to structural velocity transfer function from node 1 to node 1 is shown in Figure 28.
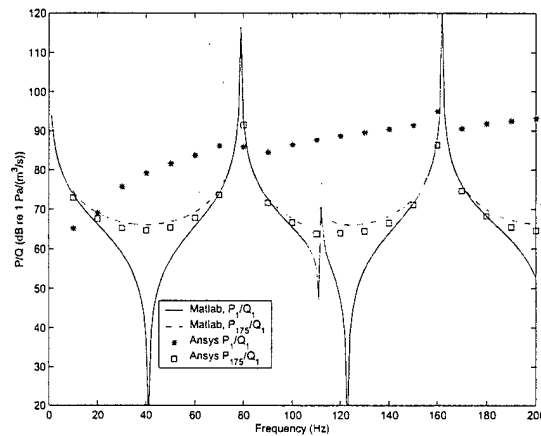
Figure 27: Acoustic impedance of the coupled system.
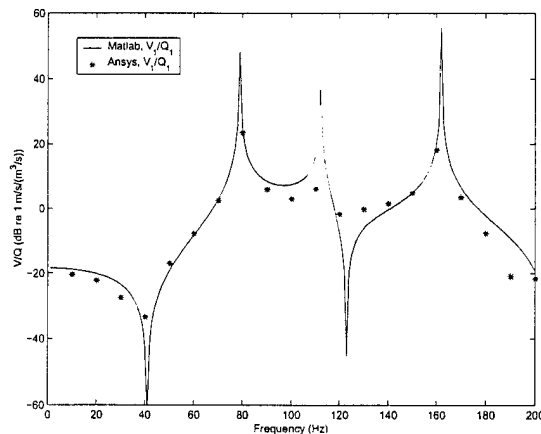
Figure 28: Structural velocity / volume velocity transfer function of the coupled system.

The poor matching between the ANSYS and MATLAB results of the point acoustic impedance in Figure 27 is to be expected. At the driving point, all modes are in phase and the stiffness residues continue to add to the system response even if the natural frequencies are several decades higher. Therefore, since the MATLAB model has a finite number of acoustic modes, the amplitude off resonance is lower than the correct ANSYS results. It should be noted that this phenomenon has no impact on the overall space averaged sound pressure level.

Comparing Figures 26 and 28 it can be seen that the transfer function between the pressure, p, at node 1 and the driving force, f, at node 1 is almost identical to the transfer function between the velocity, v, at node 1 and the volume velocity, q, at node 1. This reciprocity is to be expected as it can be shown that[6]

$$\frac{p(\vec{r}_p)}{f(\vec{r}_s)} = -\frac{v(\vec{r}_s)}{q(\vec{r}_p)} \tag{52}$$

where $\vec{r}_p$ and $\vec{r}_s$ are the position vectors in the cavity and structure respectively.

A.3 Coupled Vibro Acoustic Devices

The calculations in Section A.2 were repeated with the VAD present to validate that the modal coupling theory still works with the doubly wetted surfaces of the VAD walls.

A.3.1 Forced Response of the Structure with Coupled Cavity and VAD

As with the coupled case without the VAD (Section A.2), the curved panel was driven with a unit force in the centre of the panel (node 1). The drive point structural impedance was calculated within ANSYS by solving the fully coupled expression given by Equation (51) and also by using the modal coupling technique in MATLAB. The results from the two techniques are shown as a drive point structural impedance and force to pressure transfer function in Figures 29 and 30 respectively.
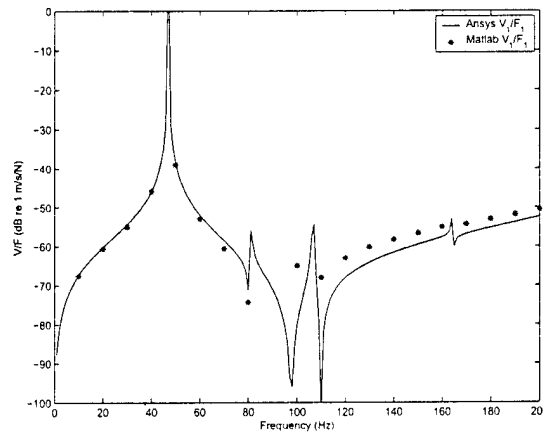
Figure 29: Drive point structural impedance of the coupled system with the VAD.

Looking at Figure 29 it is clear that the modal coupling theory accurately predicts the behaviour of the coupled system. The resonances from the two simulations are well aligned. The slight discrepancies seen at the anti-resonances are to be expected, particularly at the high frequency end, and they are due to an inadequate number of structural and/or acoustic modes used for the simulation within MATLAB. It should also be noted that due to the long time taken for the simulations within ANSYS, the frequency spacing is coarse (10 Hz) and subsequently the magnitudes near the resonances are not necessarily accurate.

Figure 30 also shows that the MATLAB simulation did not have sufficient modes to model the residues from the higher order modes. This is not such an issue for noise control simulations as the regions around the anti-resonances contribute very little to the overall energy transmission from one subsystem to another.
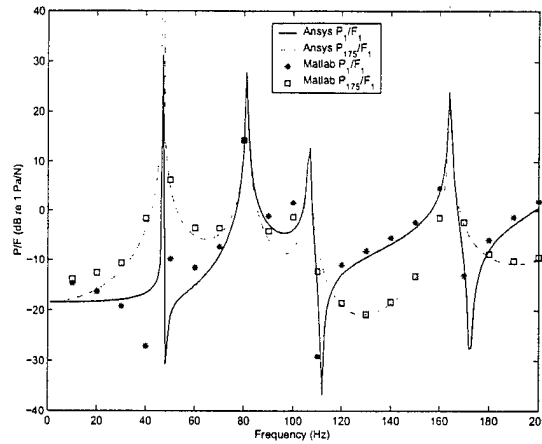
Figure 30: Pressure / Force transfer function of the coupled system with the VAD.

A.3.2　Forced Response of the Cavity with Coupled Structure and VAD

As with the coupled case without the VAD, the cavity was driven at the centre of the panel surface (at node 1) with a unit volume velocity. The system response was calculated within ANSYS by solving the fully coupled expression given by Equation 51 and also by using the modal coupling technique in MATLAB. The results from the two techniques are shown as acoustic impedances between nodes 1 and 175 to node 1, and a volume velocity to structural velocity transfer function from nodes 1 to node 1 in Figures 31 and 32 respectively.
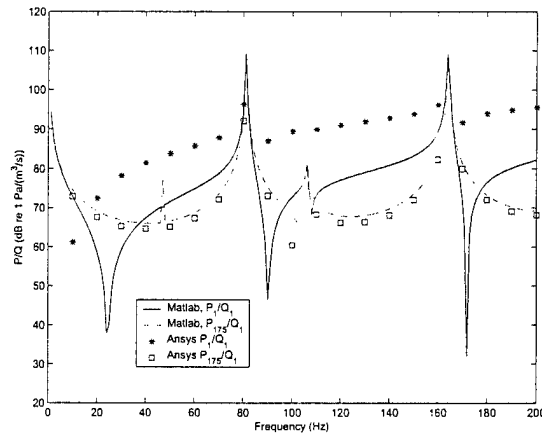
Figure 31: Acoustic impedance of the coupled system with the VAD.

　　　Comparing Figures 30 and 32 it can be seen that the transfer function between the pressure, p, at node 1 and the driving force, f, at node 1 is almost identical to the transfer function between the velocity, v, at node 1 and the volume velocity, q, at node 1. This reciprocity is to be expected as it can be shown that[6]

$$\frac{p(\vec{r}_p)}{f(\vec{r}_s)} = -\frac{v(\vec{r}_s)}{q(\vec{r}_p)} \qquad (53)$$

where $\vec{r}_p$ and $\vec{r}_s$ are the position vectors in the cavity and structure respectively.
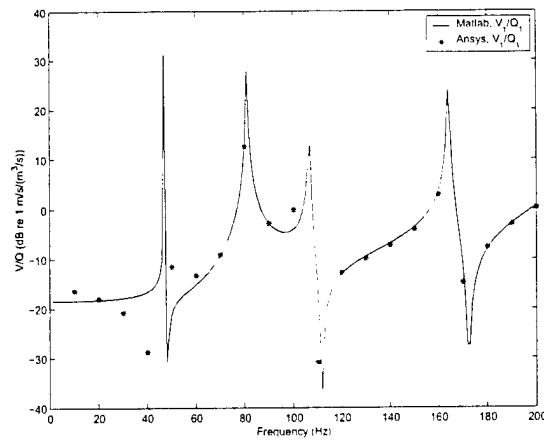
Figure 32: Structural velocity / volume velocity transfer function of the coupled system with the VAD.

A.4 Comments

From the results of the simulations for the coupled and uncoupled models it can be concluded that the modal coupling software within MATLAB is producing valid results within the limits of the theory. It shows clearly that for a coupled analysis many more modes are required for accurate prediction of the forced response off resonance, than is typical for an uncoupled model. In addition, it has been shown that for a typical coupled structural-acoustic system the modal coupling approach provides an accurate method for analysing the system response.

B   Verification of COMET

This appendix describes the numerical models constructed to validate the use of COMET to analyse acoustic scattering. Numerical results are presented for an analysis of scattering from a sphere, a simple model with a known analytical solution. Several types of Boundary Element Analyses (BEA) were evaluated and it was found that a direct method gave the best results for surface pressure.

B.1   Problem specification

A sphere of radius $\mathbf{a}$ is incident with a plane wave (pressure amplitude $\mathbf{p_0} = 1\text{Pa}$, wavenumber $k = 8$, ie 438Hz in air) travelling from left to right as shown in Figure 33.
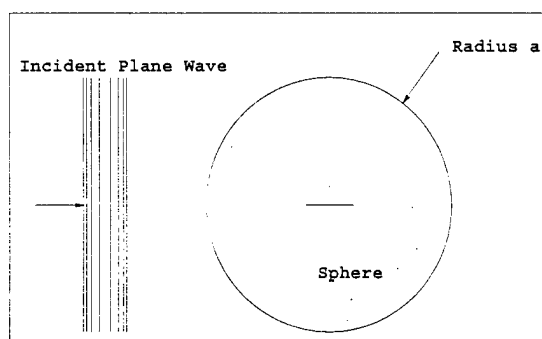
Figure 33: Schematic of the incident sound field on a sphere.

B.2   Analytical solution

An analytical solution to the problem is given in Morse and Ingard[18], Section 8.2. A MATLAB program was produced to calculate the analytical solution.

B.3   Comet solution

COMET[15] has a number of different techniques available to solve acoustic problems, but only BEA was considered in this study. Two methods are available to solve BEA problems, the "direct" and the "indirect" method.

The direct method solves for one side of the domain, and solves directly for velocity and pressure as primary variables. The indirect method solves for both sides of the domain and has the difference in pressure and the difference in pressure gradient (velocity) as primary variables. As an example, an indirect analysis of a rectangular plate sitting in free space could be solved with a 2D plate with "sharp edged" geometry, whereas a direct analysis would be of a very thin rectangular prism, i.e. a volume with thickness and direction (internal or external). A more detailed explanation of the differences between "direct" and an "indirect" BEA method is available in the COMET Users Guide[15].

Other solution parameters that can be specified include the number of elements per wavelength (**spc**), quadrature order (**qorder**) or integration accuracy, and whether you want to solve with an over-determined system of equations (direct method only). This last method is called CHIEF (**chf**) or SuperCHIEF (**schf**) and is used to suppress spurious results in an external

radiation problem at frequencies related to the internal modes. This is a purely numerical phenomenon, and is discussed in the COMET Users Guide[15] (Chapter 16 of the Examples).

Both harmonic and transient results can be calculated using COMET. In this report we only consider harmonic solutions. The system of equations must be solved at each frequency in the required range of frequencies. You cannot calculate modal solutions with the current version of COMET (4.0).

B.4 Results

Verification analyses were completed to examine:

- the direct and indirect methods,

- to determine the required number of elements per wavelength,

- to compare quadrature order,

- to examine if the method is suitable over the frequency range of interest,

- to determine the effect of the CHIEF method.

These results can be compared to the analytical solutions.

All of the below results report the magnitude of the surface pressure (the sum of the incident and scattered pressure) on the sphere from the incident plane wave. The plane wave hits the sphere at $\pm 180°$, so $0°$ is at the "rear" of the sphere.

B.4.1 Direct vs. indirect
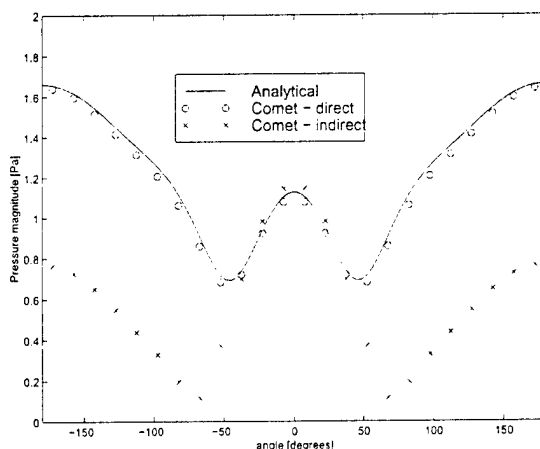
Figure 34: Comparison of analytical and calculated surface pressure over a sphere using direct and indirect BEM.

The comparison of the surface (elemental) pressures of the direct and indirect method shows very poor results for the indirect method (see Figure 34). The results shown in Figure 34 were calculated with spc=12 and qorder=1.

A possible reason for the poor results for the indirect method may be that the pressure results are a post-processing operation for the indirect method, whereas they are directly solved for by the direct method. COMET user support has been contacted on this point.

Away from the surface, on the data recovery mesh, the results are much better. Figures 37a-c show a direct, indirect and analytical (MATLAB) calculation. All appear to give similar results.


```
COMET        Database : direct_0.25_10_q1.cdb
             Results  : direct_0.25_10_q1.rslt
```

```
1.60000E+000
1.47692E+000
1.35385E+000
1.23077E+000
1.10769E+000
9.84615E-001
8.61538E-001
7.38462E-001
6.15385E-001
4.92308E-001
3.69231E-001
2.46154E-001
1.23077E-001
0.00000E+000
```

```
Acoustic Pressure, Magnitude  Frequency 437.99 Hz
COMET/Vision Ver 4.0 Mon Sep 04 12:57:45 2000
```
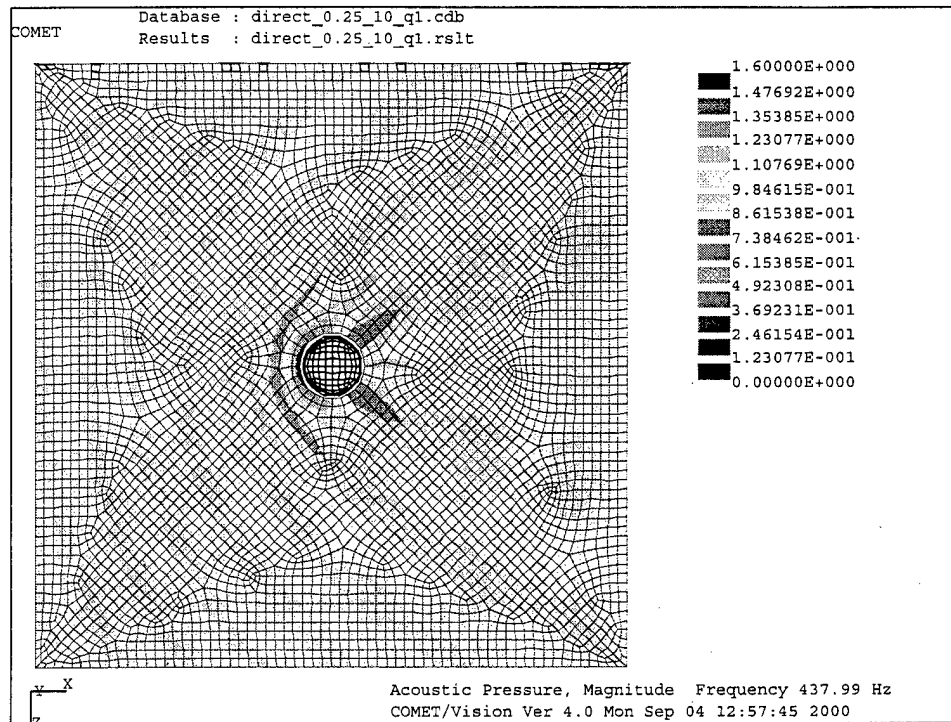
(a) Direct Method

Figure 35: Acoustic pressure field (magnitude) of scattering from a cylinder, ka=8 : Direct BEM

The direct method appears to be superior given the requirement of accurate surface pressure. However, the indirect method has an iterative solver and frequency interpolation, which may be advantageous for speeding up larger models. This may be an alternative if the surface pressure accuracy limitation could be overcome.

B.4.2 Elements per wavelength

The results presented in Figure 38 show that the 12 elements/wavelength results give a reasonably accurate solution. Depending on the accuracy of the experimental boundary conditions, 6 or 8 elements/wavelength may also be deemed acceptable for our requirements.
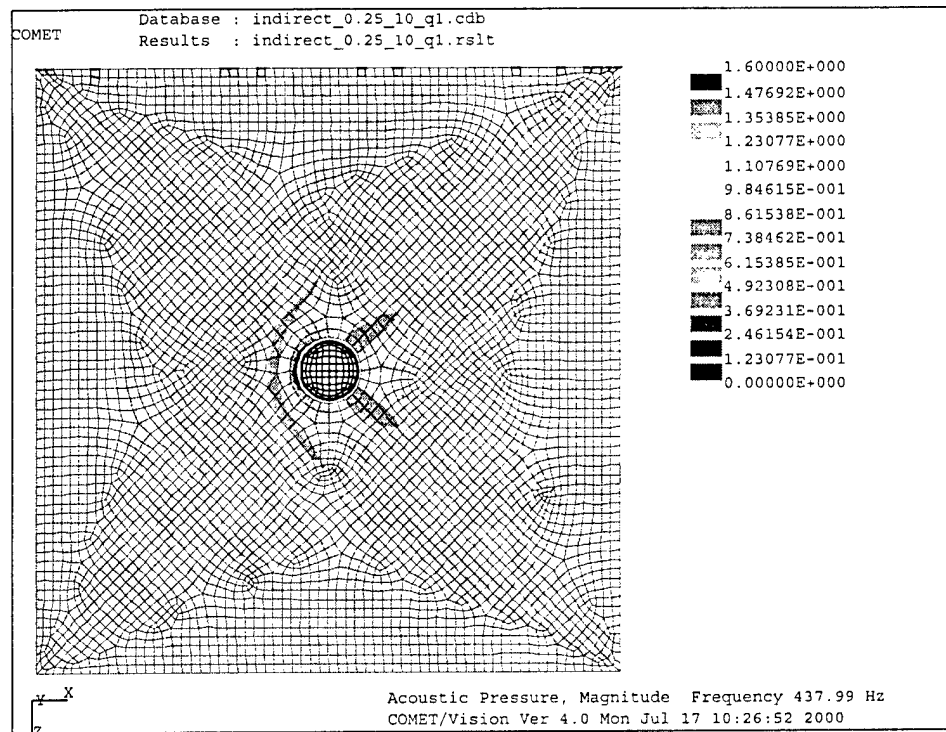
Figure 36: Acoustic pressure field (magnitude) of scattering from a cylinder, ka=8 : Indirect BEM
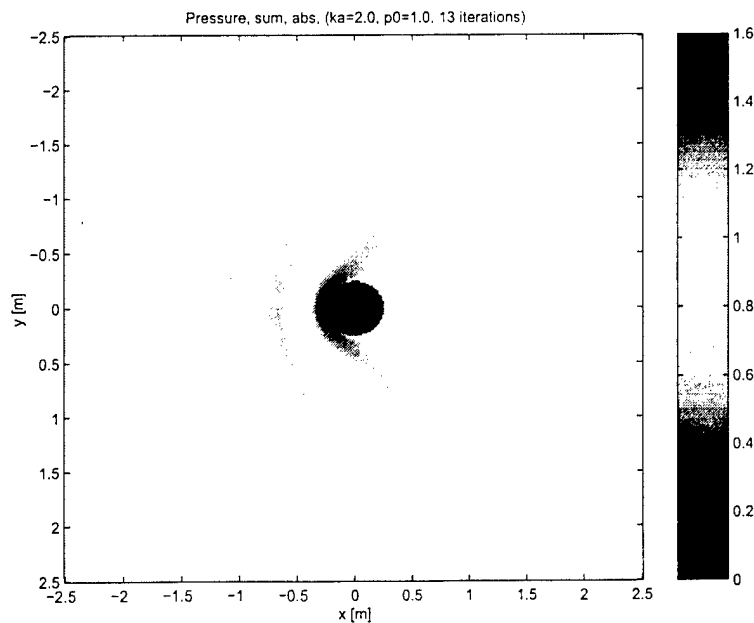
Figure 37: Acoustic pressure field (magnitude) of scattering from a cylinder, ka=8 : Matlab solution
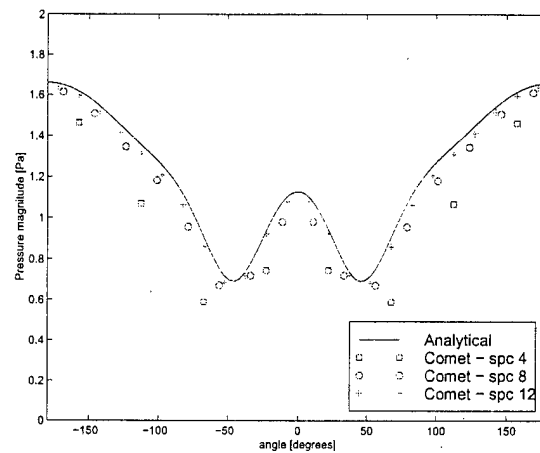
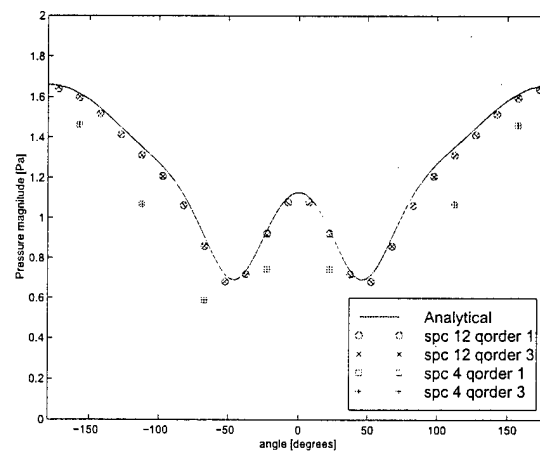Figure 38: Comparison of analytical and calculated surface pressure over a sphere for different element densities.

Figure 39: Comparison of analytical and calculated surface pressure over a sphere for different quadrature orders.

B.4.3 Quadrature order

The results presented in Figure 39 show very little difference in accuracy between changing quadrature order from 1 (least accurate) to 3 (most accurate) for both element densities.

B.4.4 Frequency range of interest

The results presented in Figure 40 show (spc=12, qorder=1) runs varying values of ka (2, 6 and 8) with excellent comparison at all values. For the current project, the frequency range of interest is up to 400Hz, and the dimensions of interest range from 0.5m to 2m. The values of ka chosen span this region of interest.

B.4.5 CHIEF and SuperCHIEF over-determination

The CHIEF and SuperCHIEF methods of over-determination are used to suppress spurious internal modes in an external problem. They were compared with analytical and normal direct methods. Seven CHIEF points were inserted inside the sphere to over-determine the problem.

The results in Figure 41 show similar calculations by the normal direct and CHIEF methods. However the SuperCHIEF results are very poor. The reasons for this are not known, and COMET user support has been contacted.

Run-times for this model using CHIEF and SuperCHIEF more than double the run-times of the normal direct method.

Figure 42 shows the pressure at a point 3m behind the sphere over a frequency range of 50-400Hz. It clearly shows the difference between the normal direct and CHIEF methods, and indicates that the CHIEF method should be used at frequencies corresponding to the internal natural modes.

B.5 Conclusion

For best results from BEM for surface pressures for an incident wave, use a direct method, element / wavelength of 12 with standard quadrature and CHIEF over-determination at frequencies corresponding to the internal natural modes. Reasonable, but less accurate, results can be obtained by using element / wavelength spacings of down to 6.
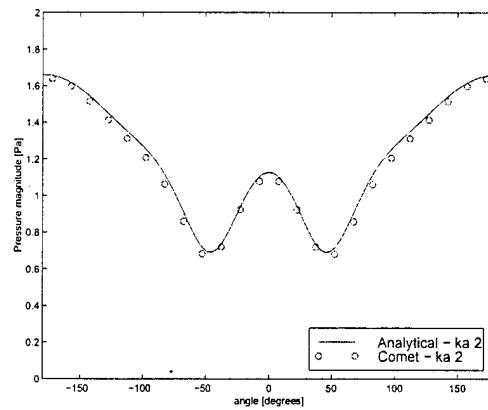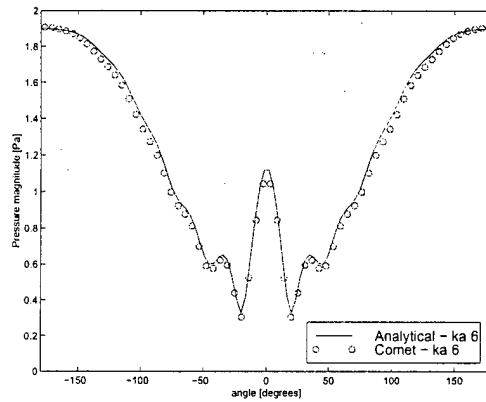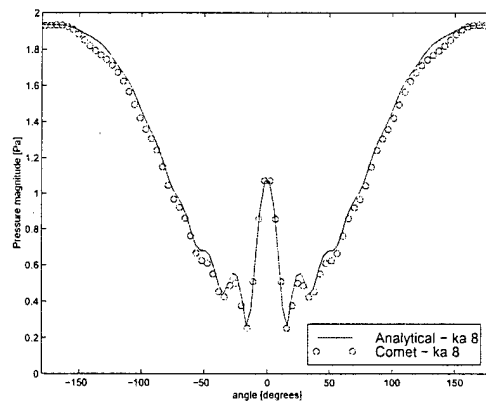
(a) ka = 2

(b) ka = 6

(c) ka = 8

Figure 40: Comparison of analytical and calculated surface pressure over a sphere for different wavenumbers.
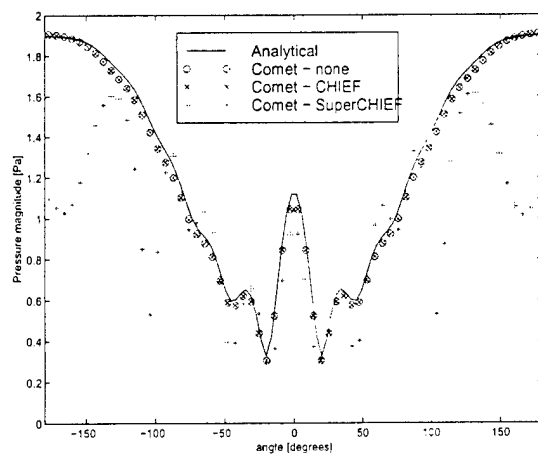
Figure 41: Comparison of analytical and calculated surface pressure over a sphere for different solution methods (namely normal direct, CHIEF and SuperCHIEF).
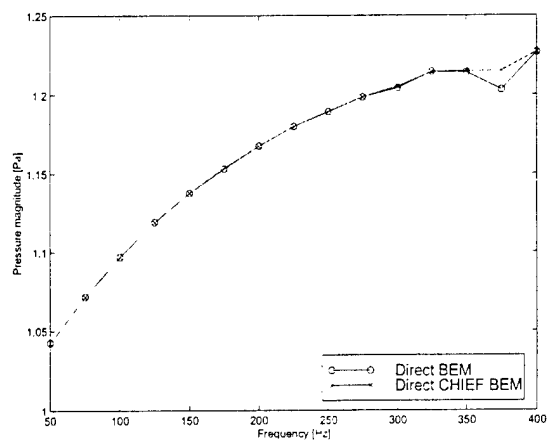

Figure 42: Comparison of the calculated surface pressure over the sphere using the direct BEM and direct CHIEF BEM as a function of frequency.

C Optimisation Results

The following section details the different configurations investigated before the more optimal designs discussed in Section 4 were achieved.

The external pressure field was generated by a monopole acoustic source located on axis 1m from the flexible panel. The results were generated in COMET at 41 frequencies and then imported into MATLAB to provide an equivalent force to all the external structural nodes. The sound field was then interpolated at all 400 frequencies, that is from 1 Hz to 400 Hz in steps of 1 Hz.

Two basic VAD configurations were investigated, the first was shown in Section 3.5.1, the other had the VAD rotated 180 degrees as shown in Figure 16.

C.1 Empty Cylinder

The effects of internal damping on the cylinder and cavity were investigated. The results of which are shown in Table 11. This can be seen in Figure 43 which plots the acoustic potential energy as a function of frequency for all 12 cases. It can be seen that damping is effective at reducing the overall sound transmission into the cavity. It does this by controlling the response primarily at resonance.

Acoustic Potential Energy (dB)	η_a				
η_s	Modal Loss Factor	2%	3.5 %	4%	8%
	2%	48.7 | 50.8	**47.6 | 49.6**	47.3 | 49.3	46.1 | 47.7
	4%	47.3 | 49.9	47.3 | 49.3	45.6 | 48.1	44.2 | 46.4
	8%	46.2 | 49.2	46.1 | 47.7	44.2 | 47.3	42.5 | 45.3

Table 11: Effects on sound transmission of internal damping in the structure and cavity. Tabulated values are the acoustic potential energy band averaged for 50 to 200 Hz and 50 to 400 Hz. The baseline configuration is shown in bold type face.

An alternative way of reducing the sound transmission is to add mass to the vibrating components.

Table 12 show the effect of adding mass (and stiffness) to the flexible aluminium panel. The mass and stiffness were added in the same proportions to keep the resonance frequencies of the panel constant. The equivalent data is shown graphically in Figure 44.

C.2 Cylinder with TMD

A tuned mass device (TMD), essentially the VAD with a very stiff diaphragm, was attached to the flexible panel at three symmetric locations at a radius of 150mm (the outer radius of the VAD). The effect on sound transmission into the cavity by the TMD can be seen in the figures below.
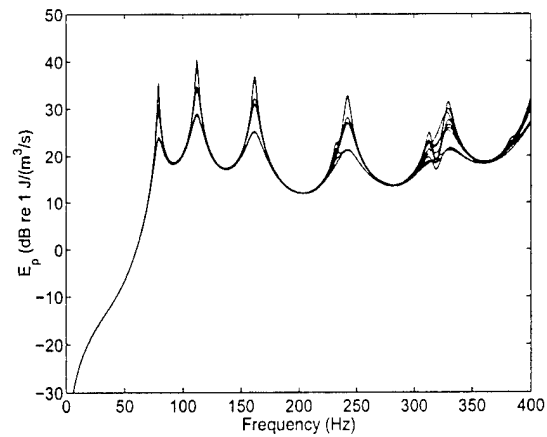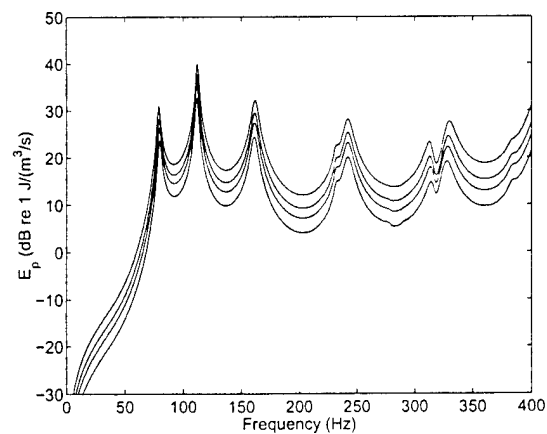
Figure 43: Effects on sound transmission of internal damping in the structure and cavity.

Additional Modal Mass (kg)	Acoustic Potential Energy (dB)
0.000	**47.6 | 49.6**
0.125	45.1 | 46.8
0.250	43.2 | 44.8
0.500	40.2 | 41.8

Table 12: Effects on sound transmission of adding mass and stiffness to the flexible panel. Tabulated values are the acoustic potential energy band averaged for 50 to 200 Hz and 50 to 400 Hz. The baseline configuration is shown in bold type face.
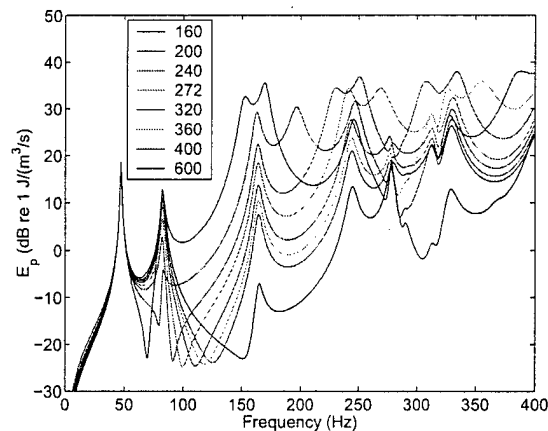

Figure 44: Effects on sound transmission of adding mass and stiffness to the flexible panel.

C.2.1 TMD resonance frequency

Table 13 and Figure 45 show the effect that modifying the resonance frequency of the TMD has on the sound transmission into the cavity.

Frequency (Hz)	Acoustic Potential Energy (dB)
160	47.5 | 48.8
200	43.1 | 47.9
240	32.9 | 51.4
272	**28.8 | 51.3**
320	24.6 | 53.0
360	30.2 | 51.4
400	30.2 | 51.4
600	29.5 | 51.4

Table 13: Effect of the TMD resonance frequency on sound transmission. Tabulated values are the acoustic potential energy band averaged for 50 to 200 Hz and 50 to 400 Hz. The baseline configuration is shown in bold type face.


Figure 45: Effect of the TMD resonance frequency on sound transmission. Uncoupled resonance frequencies range from 160 Hz to 600 Hz.

C.2.2 TMD damping

Table 14 and Figure 46 show the effect that modifying the damping of the TMD has on the sound transmission into the cavity.

Damping, η %	Acoustic Potential Energy (dB)
2	28.8 | 53.6
6	**28.8 | 51.8**
10	28.7 | 50.1
15	28.6 | 49.0
20	28.5 | 48.1

Table 14: Effect of the TMD damping on sound transmission. Tabulated values are the acoustic potential energy band averaged for 50 to 200 Hz and 50 to 400 Hz. The baseline configuration is shown in bold type face.
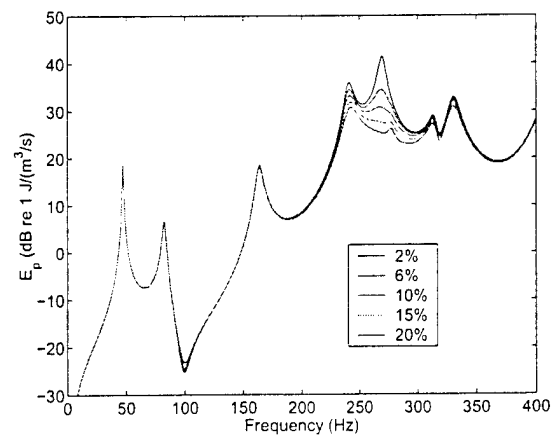

Figure 46: Effect of the TMD damping (modal loss factor) on sound transmission.

C.2.3   TMD mass

Table 15 and Figure 47 show the effect that modifying the modal mass of the TMD has on the sound transmission into the cavity. It should be noted that the resonance frequency of both the in-phase and out-of-phase modes for the panel/TMD remained unchanged.

Mass (%)	Acoustic Potential Energy (dB)
25	32.3 | 54.4
50	30.9 | 53.2
100	**28.8 | 51.3**
150	27.2 | 49.8
200	25.9 | 48.5
400	22.3 | 44.9

Table 15: Effect of the TMD (modal) mass on sound transmission. Tabulated values are the acoustic potential energy band averaged for 50 to 200 Hz and 50 to 400 Hz. The baseline configuration is shown in bold type face.
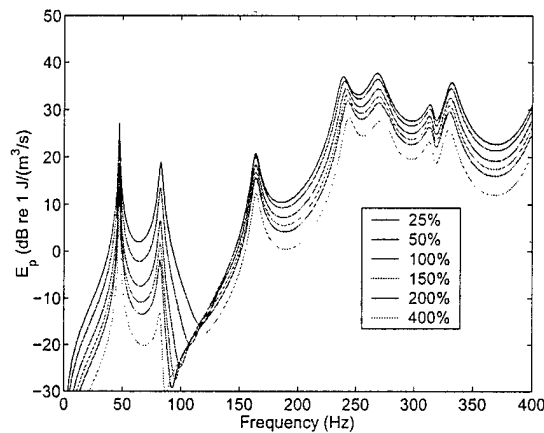

Figure 47: Effect of the TMD (modal) mass on sound transmission.

C.3   Cylinder with VAD

The diaphragm constraint was removed so that the diaphragm was allowed to move freely relative to the VAD body. The attachment points were the same for the TMD. The effect on sound transmission into the cavity by the VAD can be seen in the figures below.

C.3.1   Diaphragm resonance frequency

Table 16 and Figure 48 show the effect that modifying the resonance frequency of the diaphragm has on the sound transmission into the cavity. The resonance frequency of the diaphragm was changed by modifying the stiffness of the diaphragm supports.

Frequency (Hz)	Acoustic Potential Energy (dB)
60	30.1 | 51.4
70	30.1 | 51.4
80	**30.1 | 51.4**
90	30.1 | 51.4
100	30.2 | 51.4
110	30.2 | 51.4
120	30.2 | 51.4
140	29.5 | 51.4
160	27.6 | 51.4
240	28.3 | 51.2

Table 16: Effect of the diaphragm resonance frequency on sound transmission. Tabulated values are the acoustic potential energy band averaged for 50 to 200 Hz and 50 to 400 Hz. The baseline configuration is shown in bold type face.
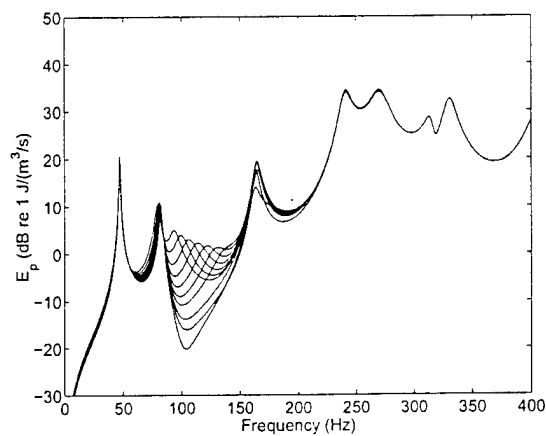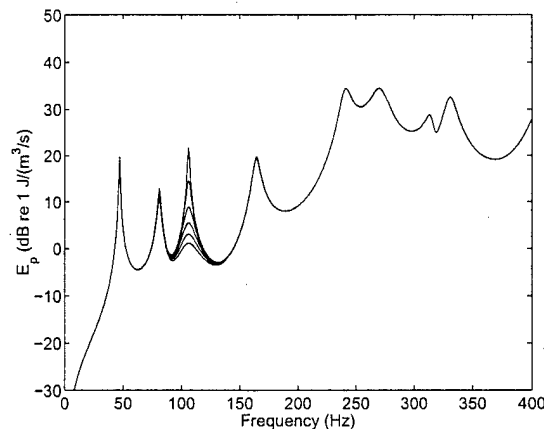

Figure 48: Effect of the diaphragm resonance frequency on sound transmission. Increasing resonance frequency moves the peak to the right.

C.3.2 Diaphragm damping

Table 17 and Figure 49 show the effect that modifying the damping of the diaphragm has on the sound transmission into the cavity.

Damping, η %	Acoustic Potential Energy (dB)
2	31.7 | 51.4
5	30.8 | 51.4
10	30.4 | 51.4
15	30.3 | 51.4
20	**30.1 | 51.4**
25	30.0 | 51.4

Table 17: Effect of the diaphragm damping (modal loss factor) on sound transmission. Tabulated values are the acoustic potential energy band averaged for 50 to 200 Hz and 50 to 400 Hz. The baseline configuration is shown in bold type face.

Figure 49: Effect of the diaphragm damping (modal loss factor) on sound transmission. Increased damping reduces the peak at resonance.

C.3.3 Diaphragm mass and stiffness

Table 18 and Figure 50 show the effect that modifying the modal mass of the diaphragm (while keeping the resonance frequency constant) has on the sound transmission into the cavity.

C.3.4 VAD resonance frequency

Table 19 and Figure 51 show the effect that modifying the resonance frequency of the VAD has on the sound transmission into the cavity.

The problem with the current TMD design is that its mass is comparable to the mass of the panel. This results is a highly coupled system, so when the panel and the TMD have similar

Modal Mass	Acoustic Potential Energy (dB)	
% of Original	With backing Cavity	W/o backing cavity
25	34.0 | 51.4	31.8 | 51.4
50	31.8 | 51.4	30.6 | 51.4
100	**30.1 | 51.4**	29.7 | 51.4
150	29.7 | 51.4	29.4 | 51.4
200	29.4 | 51.4	29.2 | 51.3
400	29.1 | 51.4	29 .0 | 51.3
800	N/A	28.9 | 51.3

Table 18: Effect of the diaphragm mass (modal mass) on sound transmission. Tabulated values are the acoustic potential energy band averaged for 50 to 200 Hz and 50 to 400 Hz. The baseline configuration is shown in bold type face.

Frequency (Hz)	Acoustic Potential Energy (dB)
160	47.4 | 48.8
200	43.5 | 48.1
240	33.8 | 51.4
272	**30.2 | 51.4**
320	26.8 | 53.1
360	25.2 | 52.4
400	24.2 | 52.2
600	22.9 | 35.6

Table 19: Effect of the VAD resonance frequency on sound transmission. Tabulated values are the acoustic potential energy band averaged for 50 to 200 Hz and 50 to 400 Hz. The baseline configuration is shown in bold type face.
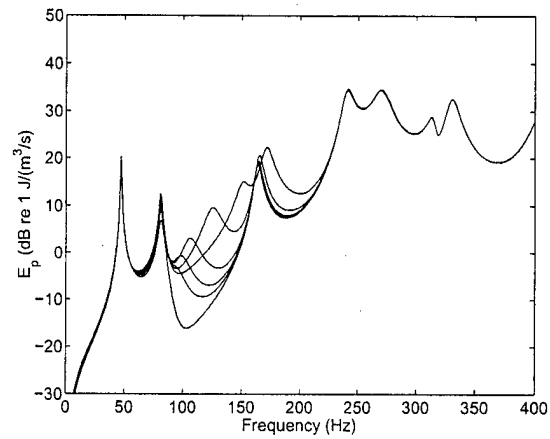
(a) With backing cavity
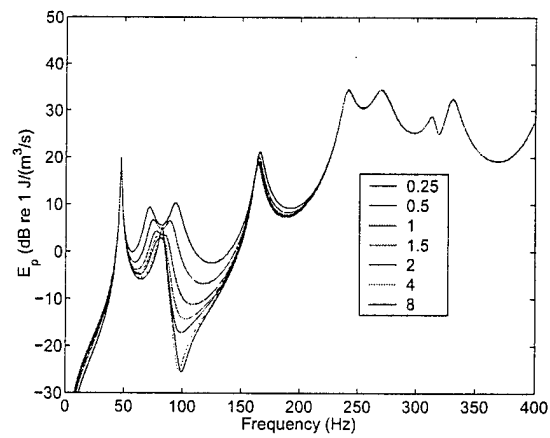
(b) Without backing cavity

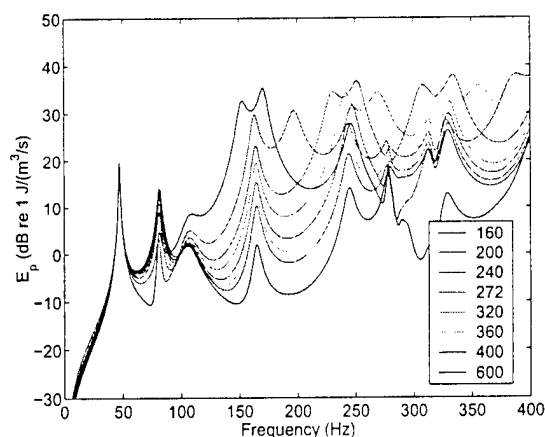Figure 50: Effect of the diaphragm mass (modal mass) on sound transmission.

Figure 51: Effect of the VAD resonance frequency on sound transmission. Uncoupled resonance frequencies range from 160 Hz to 600 Hz.

uncoupled resonance frequencies, the coupled system results in one mode with a lower natural frequency and another mode with a higher natural frequency than the original natural frequencies. The overall broadband impedance of the final coupled system is not significantly reduced, and is only really reduced by the mass effects of the TMD. The only solution is to try and push the two modes outside the frequency band of interest by mass loading the in-phase panel mode and stiffness load the out-of-phase panel mode.

C.3.5 VAD damping

Table 20 and Figure 52 show the effect that modifying the damping of the VAD has on the sound transmission into the cavity.

Damping, η %	Acoustic Potential Energy (dB)
2	30.2 | 53.6
6	**30.1 | 51.4**
10	30.1 | 50.2
15	30.0 | 49.1
20	29.9 | 48.2

Table 20: Effect of the VAD damping on sound transmission. Tabulated values are the acoustic potential energy band averaged for 50 to 200 Hz and 50 to 400 Hz. The baseline configuration is shown in bold type face.

C.3.6 VAD Mass

Table 21 and Figure 53 show the effect that modifying the modal mass of the VAD has on the sound transmission into the cavity. It should be noted that the resonance frequency of both the in-phase and out-of-phase modes for the panel/VAD remained unchanged.
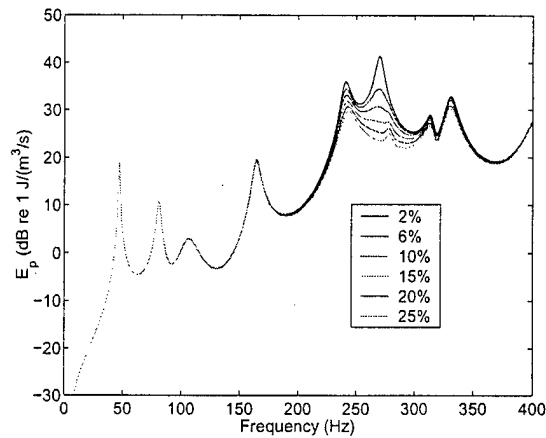
Figure 52: Effect of the VAD damping (modal loss factor) on sound transmission.

Mass (%)	Acoustic Potential Energy (dB)
25	32.9 | 54.1
50	31.8 | 53.1
100	**30.1 | 51.4**
150	28.9 | 50.0
200	27.9 | 48.8
400	25.4 | 45.3

Table 21: Effect of the VAD (modal) mass on sound transmission. Tabulated values are the acoustic potential energy band averaged for 50 to 200 Hz and 50 to 400 Hz. The baseline configuration is shown in bold type face.
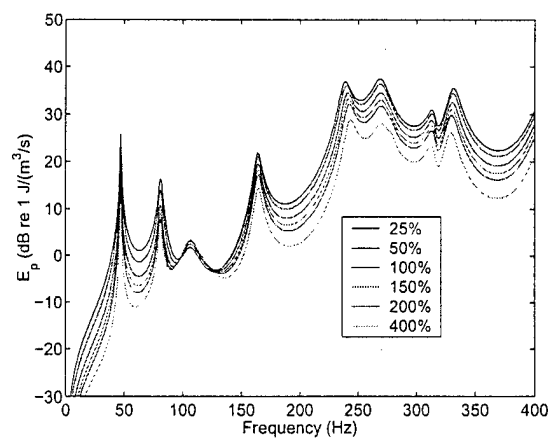

Figure 53: Effect of the VAD (modal) mass on sound transmission.

C.4   Cylinder with Reversed VAD

The orientation of the VAD was reversed so that the diaphragm faced the flexible panel. The attachment points were the same as for the previous cases. The effect on sound transmission into the cavity by the VAD can be seen in the figures below.

C.4.1   Reversed VAD Diaphragm resonance frequency

Table 22 and Figure 54 show the effect that modifying the resonance frequency of the diaphragm has on the sound transmission into the cavity. The resonance frequency of the diaphragm was changed by modifying the stiffness of the diaphragm supports.

Frequency (Hz)	Acoustic Potential Energy (dB)
60	26.9 | 50.7
70	26.6 | 50.7
80	**26.3 | 50.7**
90	26.0 | 50.6
100	25.7 | 50.6
110	25.3 | 50.6
120	25.0 | 50.6
140	25.2 | 50.5
160	27.8 | 50.4
240	29.3 | 49.6

Table 22: Effect of the reversed VAD diaphragm resonance frequency on sound transmission. Tabulated values are the acoustic potential energy band averaged for 50 to 200 Hz and 50 to 400 Hz. The baseline configuration is shown in bold type face.

C.4.2   Reversed VAD Diaphragm damping

Table 23 and Figure 55 show the effect that modifying the damping of the diaphragm has on the sound transmission into the cavity.

C.4.3   Reversed VAD Diaphragm mass and stiffness

Table 24 and Figure 56 show the effect that modifying the modal mass of the diaphragm (while keeping the resonance frequency constant) has on the sound transmission into the cavity.

C.4.4   Reversed VAD resonance frequency

Table 25 and Figure 57 show the effect that modifying the resonance frequency of the reversed VAD has on the sound transmission into the cavity.
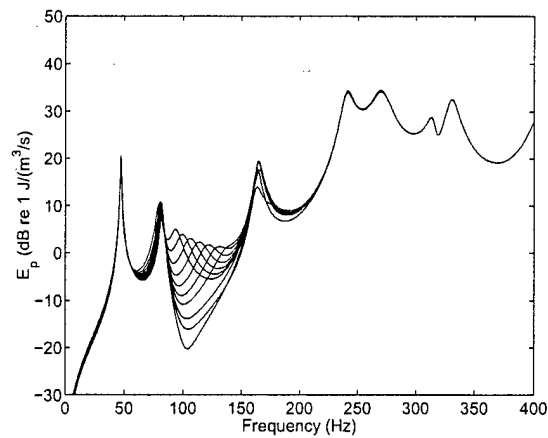
Figure 54: Effect of the reversed VAD diaphragm resonance frequency on sound transmission. Increasing resonance frequency moves the peak to the right.

Damping, η %	Acoustic Potential Energy (dB)
2	29.2 | 50.7
5	27.8 | 50.7
10	26.9 | 50.7
15	26.5 | 50.7
20	**26.3 | 50.7**
25	26.2 | 50.6

Table 23: Effect of the reversed VAD diaphragm damping (modal loss factor) on sound transmission. Tabulated values are the acoustic potential energy band averaged for 50 to 200 Hz and 50 to 400 Hz. The baseline configuration is shown in bold type face.
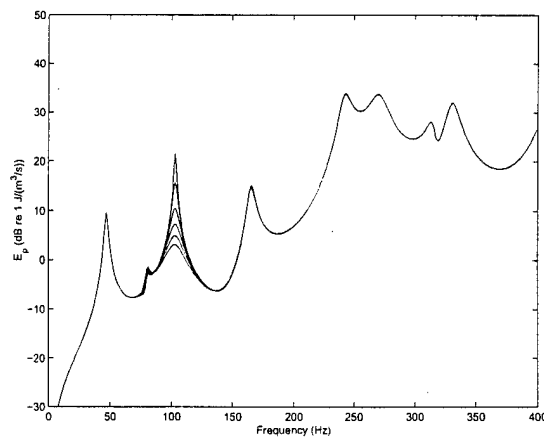

Figure 55: Effect of the reversed VAD diaphragm damping (modal loss factor) on sound transmission. Increased damping reduces the peak at resonance.

Modal Mass % of Original	Acoustic Potential Energy (dB)
25	30.6 | 49.6
50	26.0 | 50.3
100	**26.3 | 50.7**
150	26.9 | 50.8
200	27.2 | 50.8
400	27.8 | 50.9

Table 24: Effect of the reversed VAD diaphragm mass (modal mass) on sound transmission. Tabulated values are the acoustic potential energy band averaged for 50 to 200 Hz and 50 to 400 Hz. The baseline configuration is shown in bold type face.
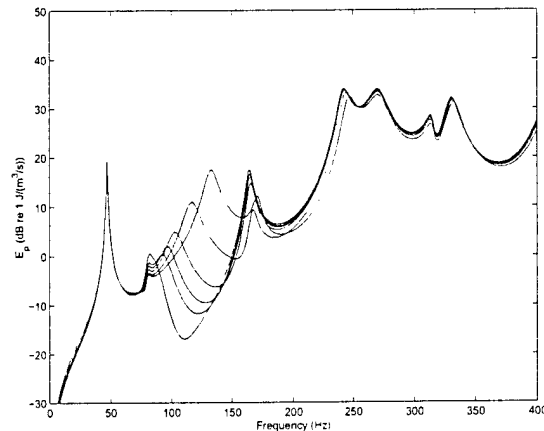

Figure 56: Effect of the reversed VAD diaphragm mass (modal mass) on sound transmission.

Frequency (Hz)	Acoustic Potential Energy (dB)
160	47.0 | 48.3
200	41.9 | 47.1
240	30.9 | 51.0
272	**26.3 | 50.7**
320	21.9 | 52.7
360	20.0 | 52.0
400	19.2 | 51.9
600	19.6 | 34.2

Table 25: Effect of the reversed VAD resonance frequency on sound transmission. Tabulated values are the acoustic potential energy band averaged for 50 to 200 Hz and 50 to 400 Hz. The baseline configuration is shown in bold type face.
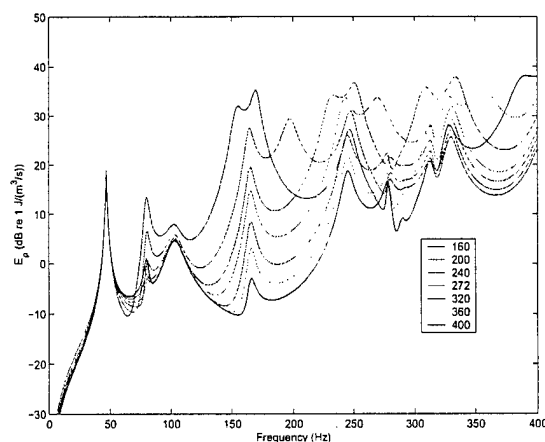
Figure 57: Effect of the reversed VAD resonance frequency on sound transmission. Uncoupled resonance frequencies range from 160 Hz to 600 Hz.

C.4.5 Reversed VAD damping

Table 26 and Figure 58 show the effect that modifying the damping of the reversed VAD has on the sound transmission into the cavity.

Damping, η %	Acoustic Potential Energy (dB)
2	26.3 | 53.0
6	**26.3 | 50.7**
10	26.3 | 49.2
15	26.2 | 48.3
20	26.2 | 47.4
25	26.1 | 46.7

Table 26: Effect of the reversed VAD damping on sound transmission. Tabulated values are the acoustic potential energy band averaged for 50 to 200 Hz and 50 to 400 Hz. The baseline configuration is shown in bold type face.

C.4.6 Reversed VAD Mass

Table 27 and Figure 59 show the effect that modifying the modal mass of the reversed VAD has on the sound transmission into the cavity. It should be noted that the resonance frequency of both the in-phase and out-of-phase modes for the panel/VAD remained unchanged.
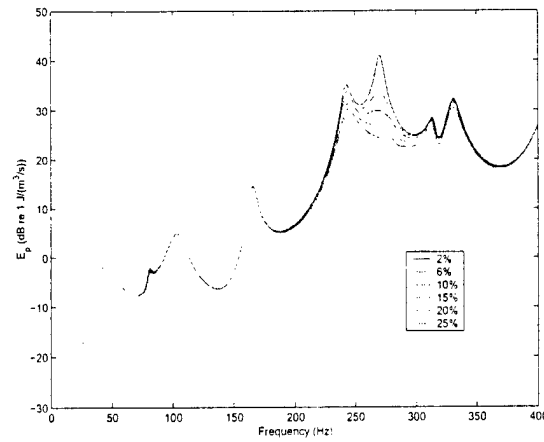
Figure 58: Effect of the reversed VAD damping (modal loss factor) on sound transmission.

Mass (%)	Acoustic Potential Energy (dB)
25	29.7 | 53.7
50	28.4 | 52.5
100	**26.3 | 50.7**
150	24.7 | 49.1
200	23.5 | 47.6
400	20.8 | 44.2

Table 27: Effect of the VAD (modal) mass on sound transmission. Tabulated values are the acoustic potential energy band averaged for 50 to 200 Hz and 50 to 400 Hz. The baseline configuration is shown in bold type face.
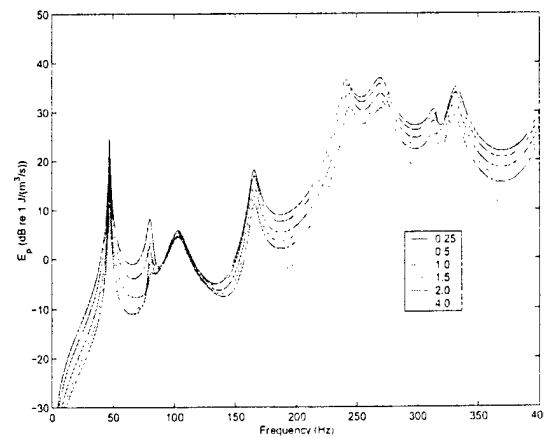

Figure 59: Effect of the reversed VAD (modal) mass on sound transmission.